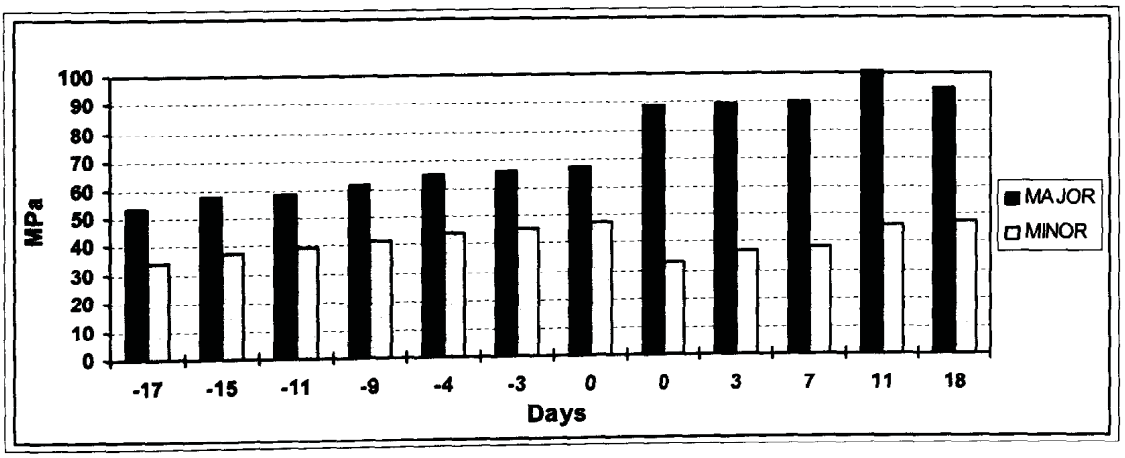

Figure 3.8.4 Principal stresses calculated from strain gauge measurements (1 m away from blasthole), Test blast 3

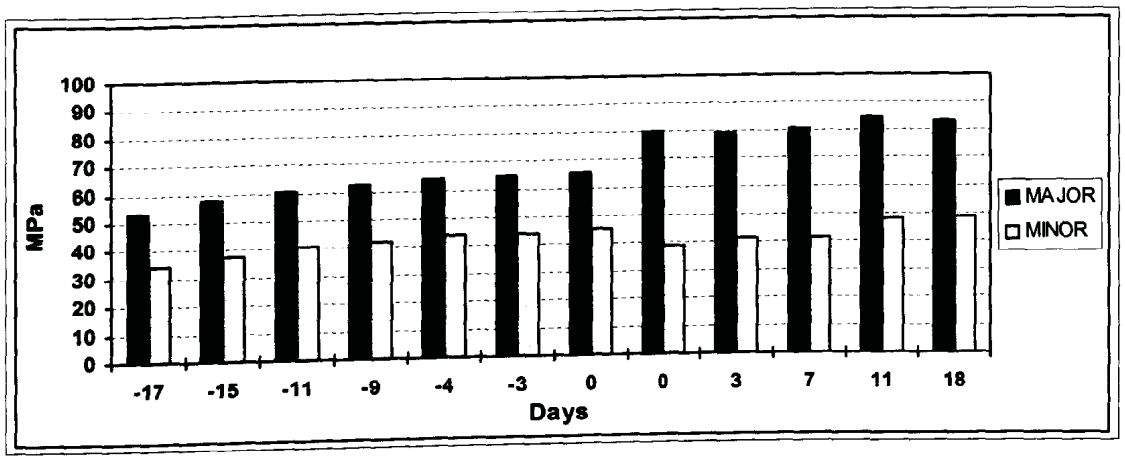

Figure 3.8.5 Principal stresses calculated from strain gauge measurements (1.5 m away from blasthole), Test blast 3

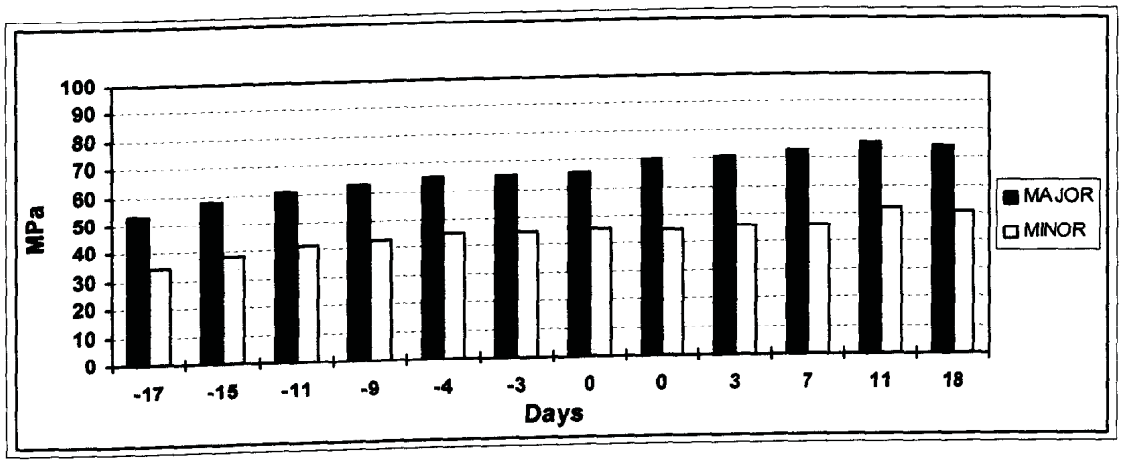

Figure 3.8.6 Principal stresses calculated from strain gauge measurements (2 m away from blasthole), Test blast 3

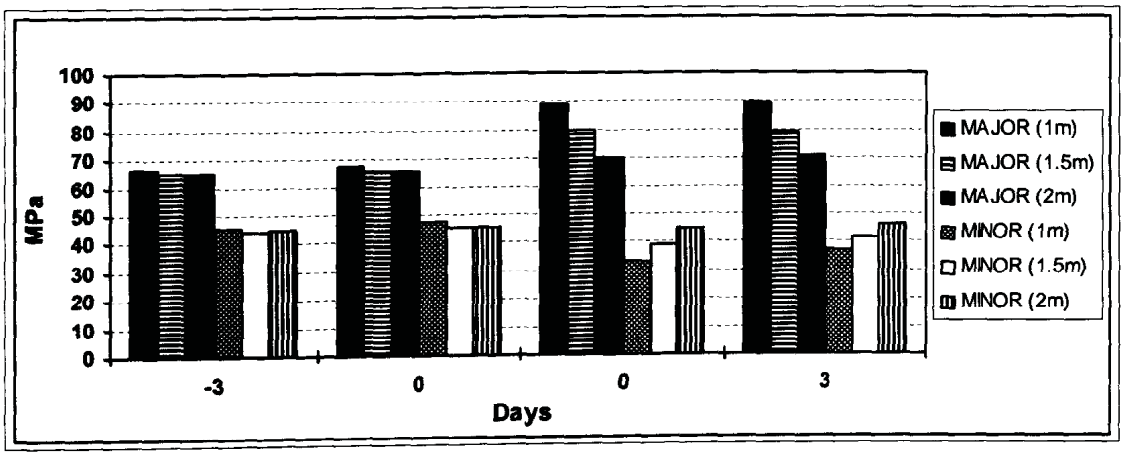

Figure 3.8.7 Principal stresses calculated from strain gauge measurements at varying distances away from blasthole, Test blast 3

In the fourth preconditioning test blast, the dynamic strain measurements were done in five boreholes which were positioned at three different depths (4 m, 5 m and 6 m). The results are presented in Figure 3.8.8 to Figure 3.8.12. In order to determine the extent of the blast effect, the distance factor (Figure 3.8.13) and the depth factor (Figure 3.8.14) were examined. The degree of the influence of the preconditioning blast decreases with distance from the blasting point. The biggest effect was observed at the closest doorstopper (Figure 3.8.8), and no significant effect was observed at the farthest one (Figure 3.8.12). The doorstoppers at 4 m and 5 m depths (Figure 3.8.9 and Figure 3.8.10) showed very similar effects but the one at 6 m (Figure 3.8.11) showed almost no effect.

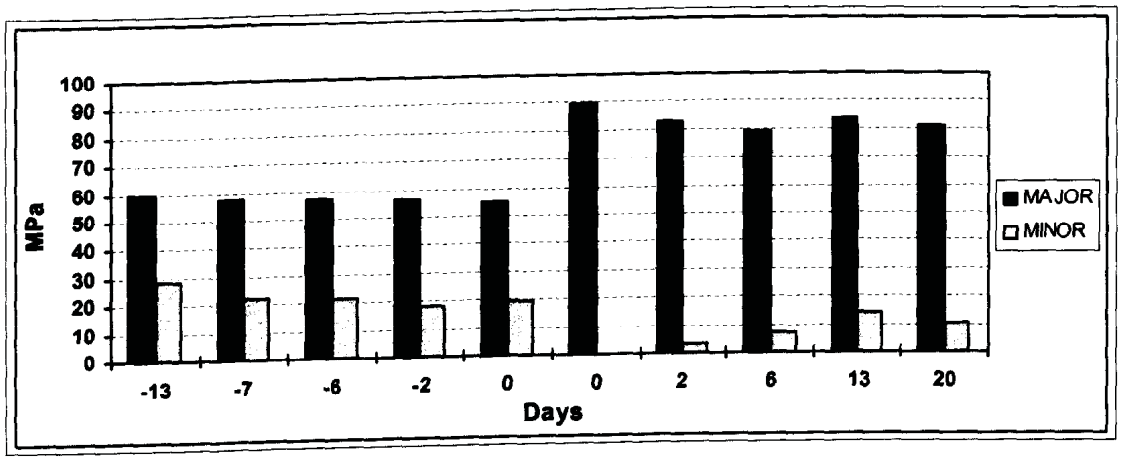

Figure 3.8.8 Principal stresses calculated from strain gauge measurements at 5 m depth (1 m away from blasthole), Test blast 4

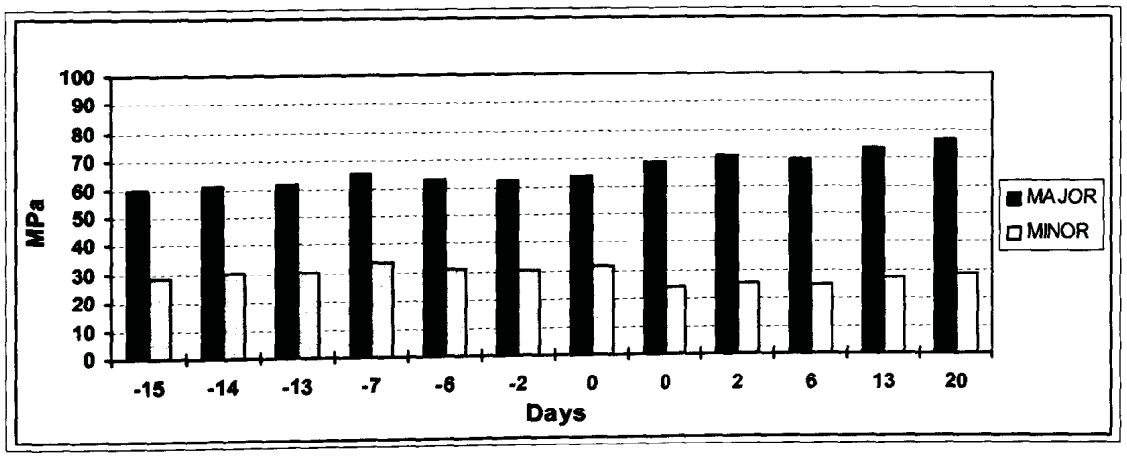

Figure 3.8.9 Principal stresses calculated from strain gauge measurements at 4 m depth (1.5 m away from blasthole), Test blast 4

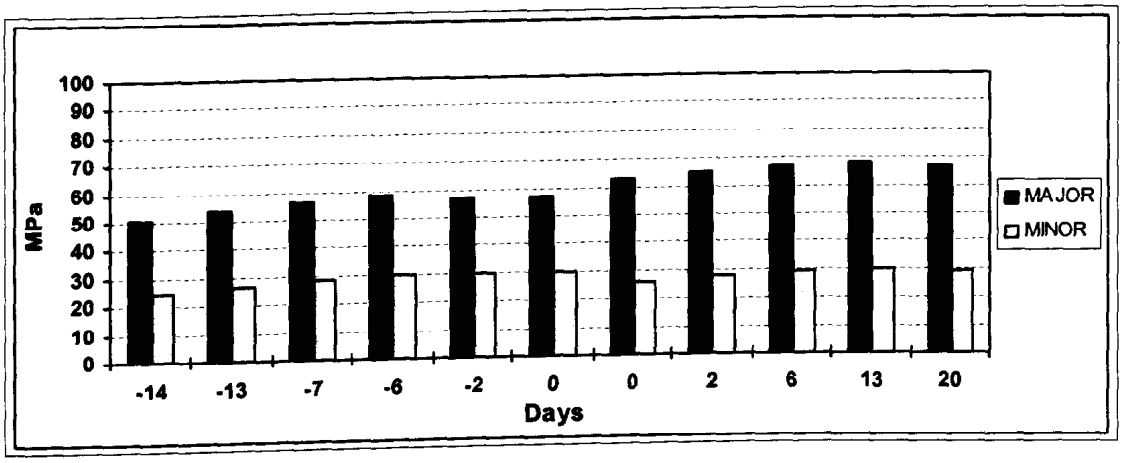

Figure 3.8.10 Principal stresses calculated from strain gauge measurements at 5 m depth (1.5 m away from blasthole), Test blast 4

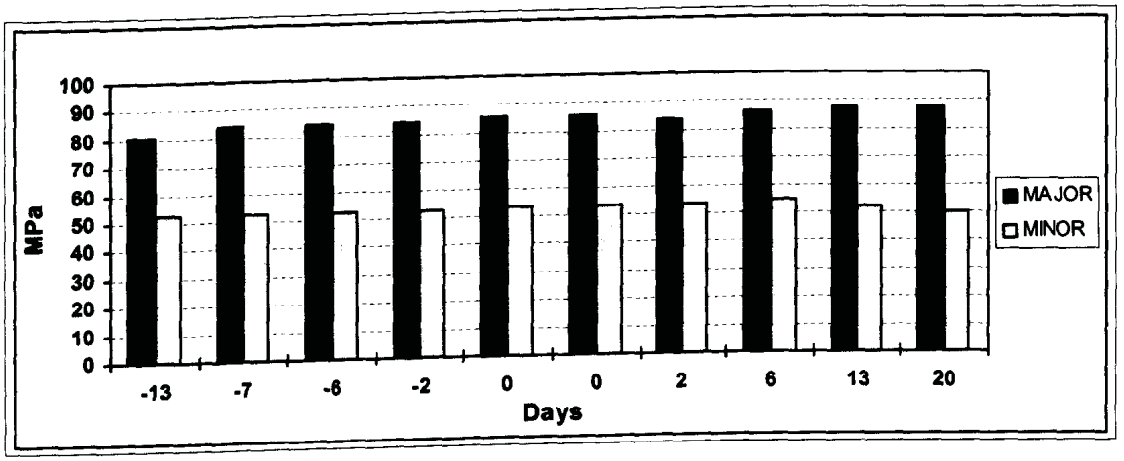

Figure 3.8.11 Principal stresses calculated from strain gauge measurements at 6 m depth (1.5 m away from blasthole), Test blast 4

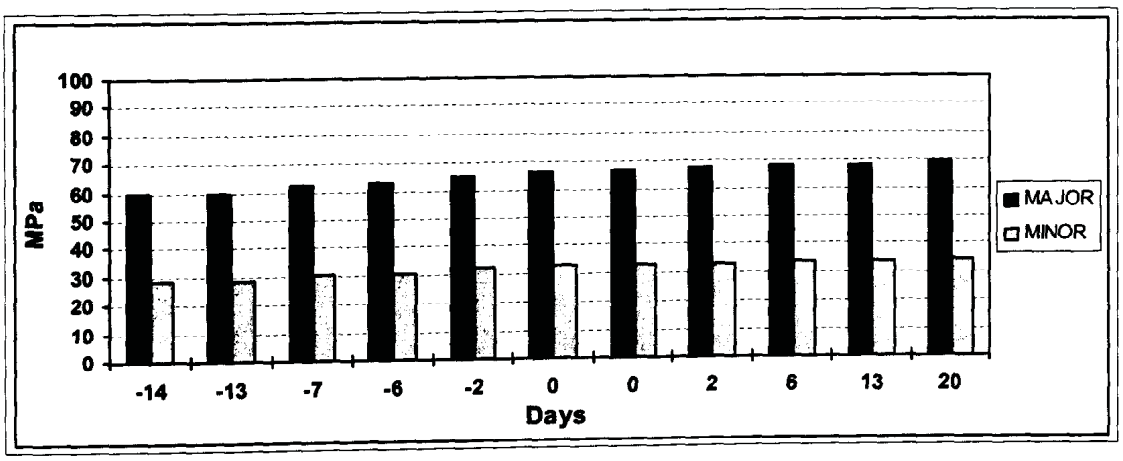

Figure 3.8.12 Principal stresses calculated from strain gauge measurements at 5 m depth (2 m away from blasthole), Test blast 4

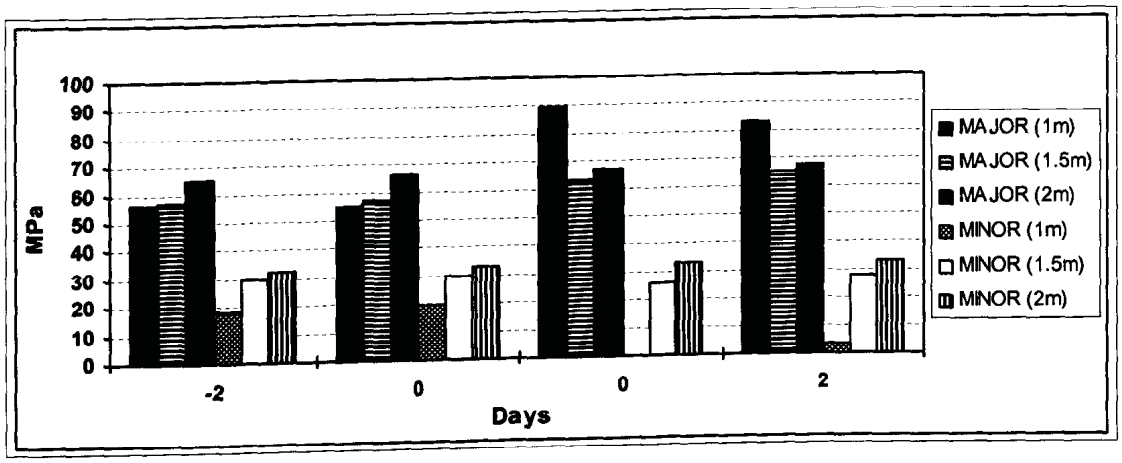

Figure 3.8.13 Principal stresses calculated from strain gauge measurements at various distances from blasthole, Test blast 4

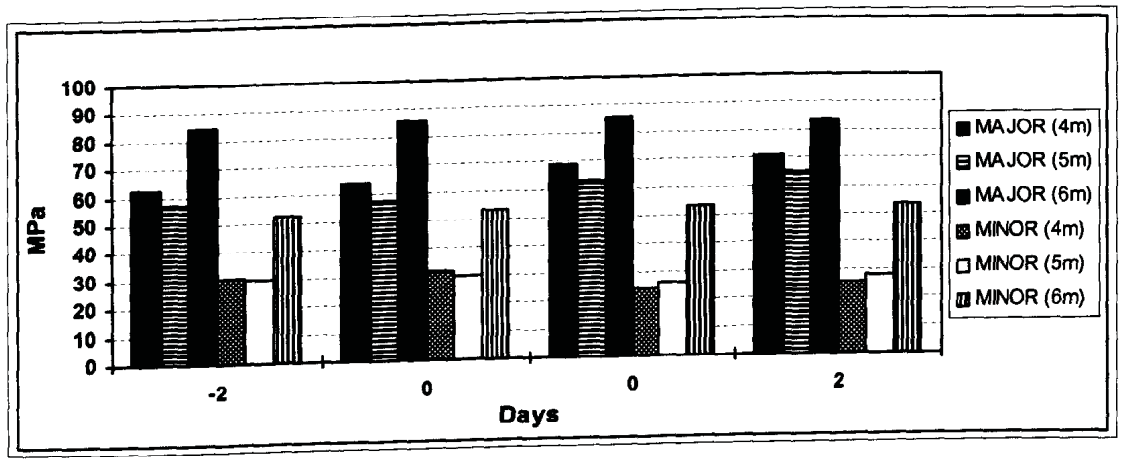

Figure 3.8.14 Principal stresses calculated from strain gauge measurements at various depths (1.5 m away from blasthole), Test blast 4

The strain gauge results confirmed the previous results, in that the major principal stresses were increased and the minor principal stresses were decreased after the preconditioning blasts had taken place.

In addition to the changes in magnitudes of principal stresses, the orientations of principal stresses were also changed subsequent to the preconditioning test blasts. An approximately 90 degrees re-orientation of the principal stress occurred in most cases of the 11 strain measurements (Figure 3.8.15 to Figure 3.8.18). The mobilisation of the bedding planes as an effect of the blast might have caused this re-orientation. The orientation of bedding planes is shown by dashed lines in these figures.

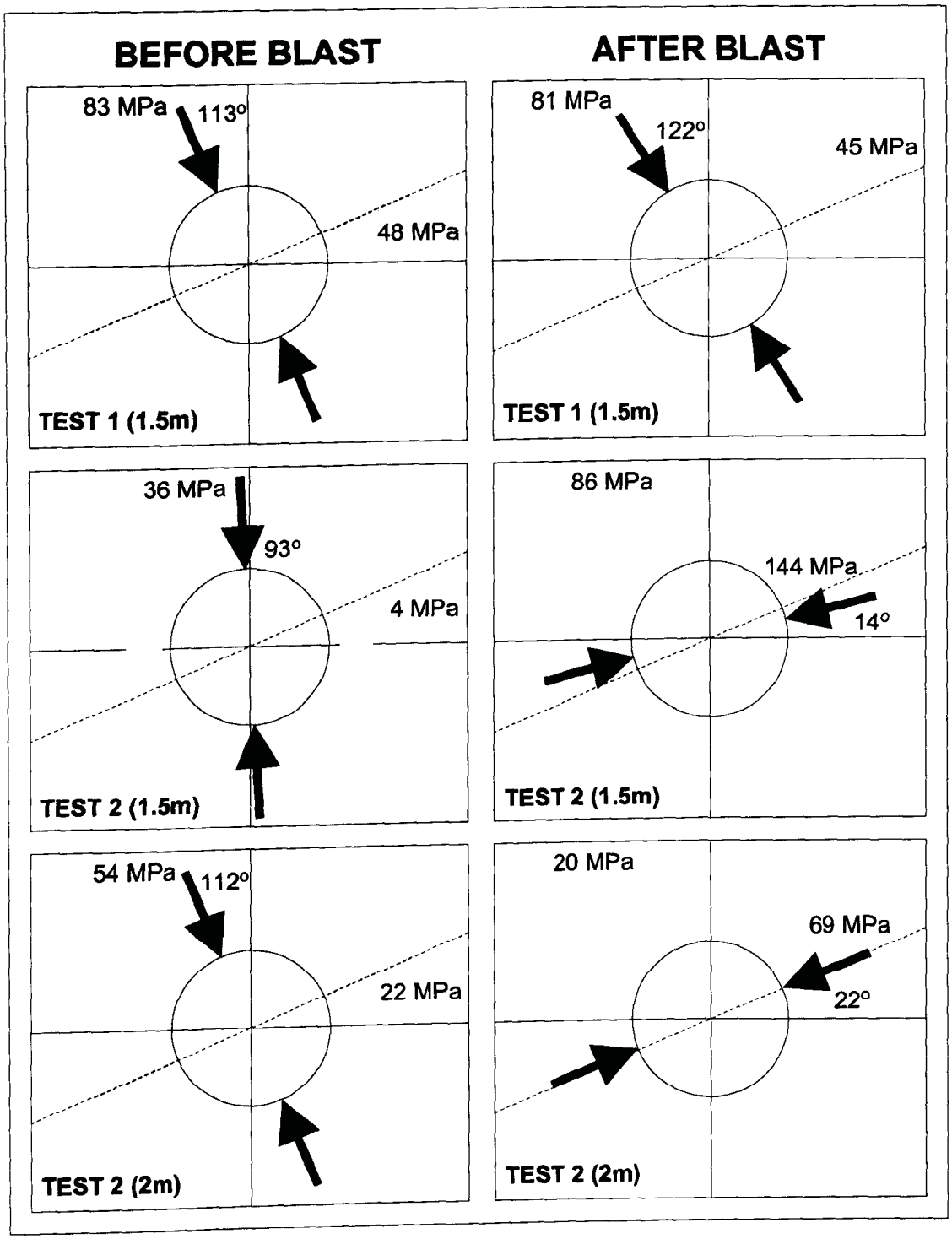

Figure 3.8.15 Orientation of principal stresses before and after test blasts 1 & 2

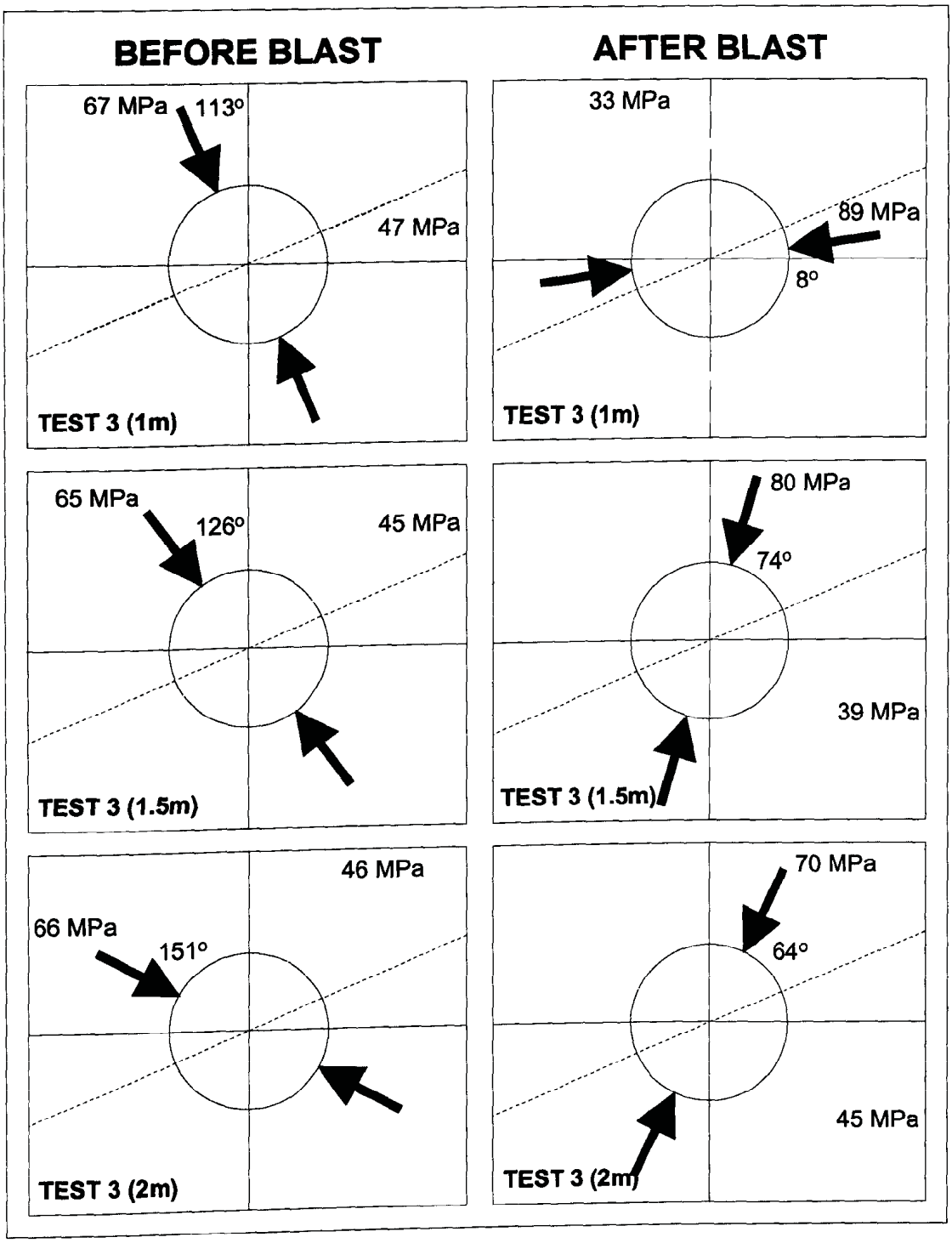

Figure 3.8.16 **Orientation of principal stresses before and after test blast 3**

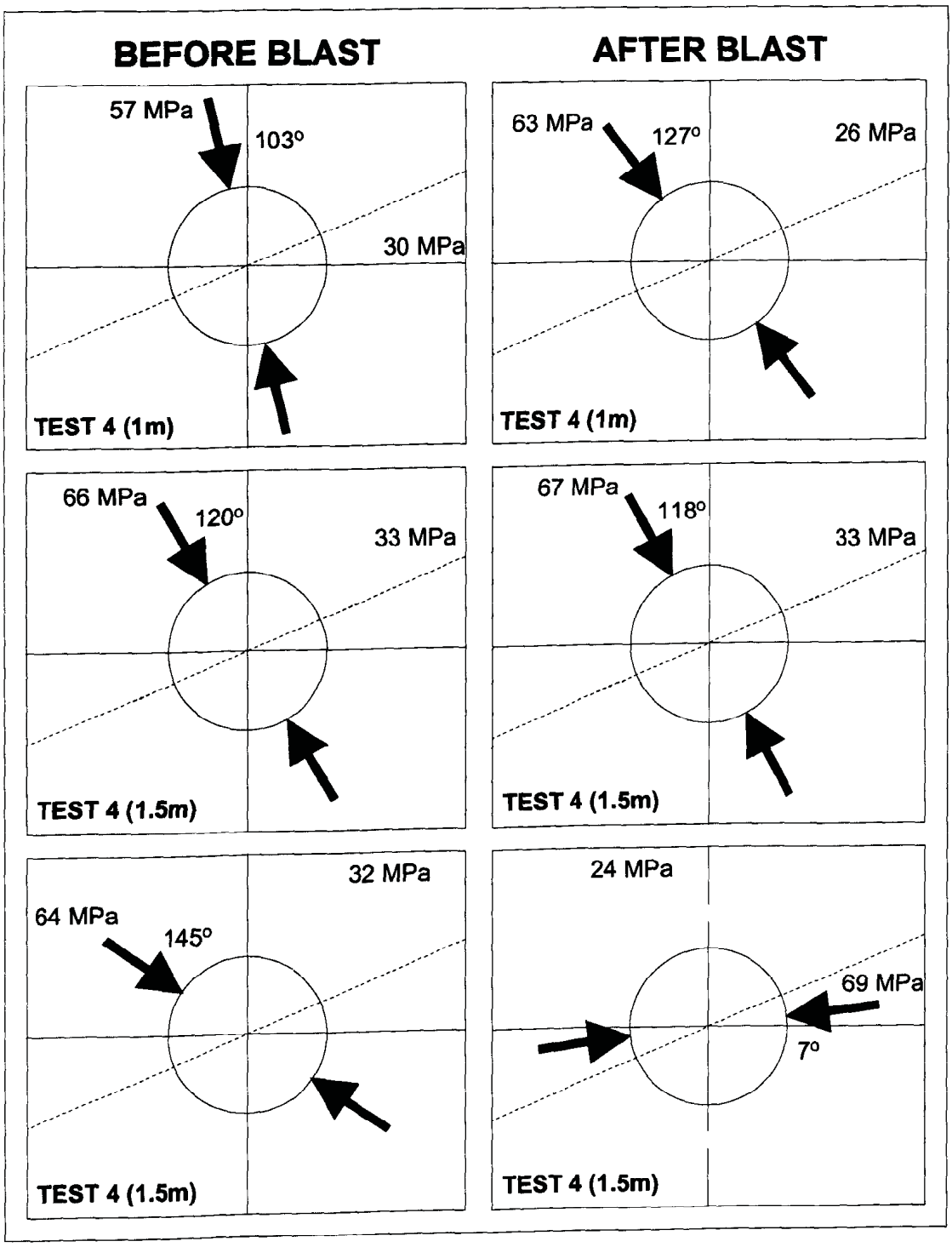

Figure 3.8.17 Orientation of principal stresses before and after test blast 4

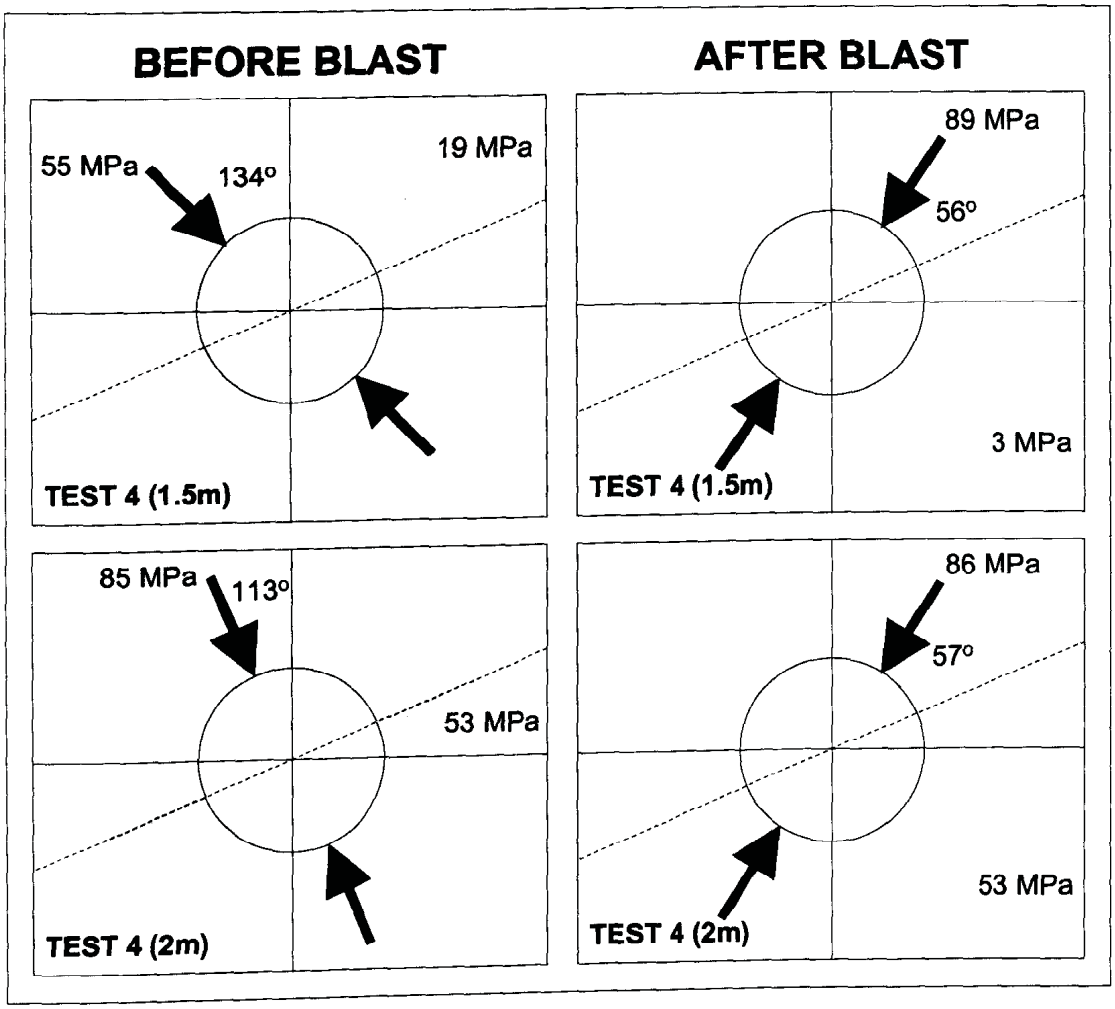

Figure 3.8.18 **Orientation of principal stresses before and after test blast 4**

3.9 Numerical modelling

The computer program DIGS (Discontinuity Interaction Growth Simulation) (Napier, 1991; Napier and Hildyard, 1992; and Napier and Pierce, 1995) was used to simulate the propagation of multiple fractures from a blasthole due to the gas pressure generated by the explosive charge. In order to do that, a two-dimensional displacement-discontinuity method was used to model a plane perpendicular to the borehole axis, in which vertical fractures may propagate.

A series of DIGS models was formulated to determine which physical parameters significantly affected the growth of the fractures and the change in field stresses in the vicinity of the blasthole. Another objective of this study was to simulate the underground experiment at West Driefontein Gold Mine and to re-evaluate the results obtained from this study and to gain an understanding of the blasting mechanism, as well as the factors involved in the process.

According to the numerical procedure for modelling the fracture growth process, each fracture is modelled as a series of displacement discontinuity boundary elements that are joined end to end to form the fracture path in an incremental growth sequence. For all models a tensile growth criterion was used. In choosing the propagation path, tensile stress values are evaluated at a fixed radius around the end of an existing discontinuity. The angle θ at which the tensile stress ahead of a crack tip is a maximum is then chosen as the growth direction. Each crack tip is advanced incrementally in the direction that maximises the specified growth criterion, and fracturing is assumed to continue from a crack tip as long as the specified failure criterion is met at the designated point ahead of the crack tip.

The blast is simulated by applying gas pressure to each of the faces of a fan of cracks emanating from a point. To avoid the complexity in description of pressure-time history for blast loading, it was assumed that all the points on the blasthole walls in contact with the entire length of charge will be loaded with the same pressure at any instant in time. Multiple fractures are checked sequentially for crack growth, and segments are added until the rupture criterion is no longer exceeded. Following the growth of fractures from the extremities of the

pressurised cracks, the blast pressure is removed from the fan and is replaced by a residual opening dilation on each crack.

Various models were run by changing the inclination of bedding planes (0, 30, 60, 90 degrees) and blast pressure (500 or 1000 MPa) The friction angle and the cohesion for the bedding planes were assumed as 30 degrees and zero respectively. All other parameters were assumed according to the field data (Table 3.9.1).

The numerical modelling (DIGS) results (Figure 3.9.1 to Figure 3.9.24) show some degree of similarity with the field observations. Longer blast-induced fractures were observed in the direction of maximum principal stress and the stress field around the blasthole was changed both in magnitude and direction.

Table 3.9.1 Parameters used for DIGS models

Field Stresses	σ_v= 100 MPa, σ_h= 50 MPa
Rock Properties	E= 71.9 GPa, ν= 0.23
Growth Elements	Un-mobilised, C=50 MPa, ϕ= 37° Mobilised, C= 0 MPa, ϕ= 37°
Bedding Planes	C= 0 MPa, ϕ= 30°, Spacing = 30 cm
Blasthole	Fan shaped 12 growth elements (Each 10 cm long)
Blast Pressure	500 or 1000 MPa

Figure 3.9.1 shows the stress field around a blasthole for the model with no bedding plane, and it is clear that the change in the orientation of the principal stresses is controlled by the stress field (i.e. the longer blast-induced fractures in the direction of major principal stress). However, in the other models with bedding planes, it seems that re-orientation of the principal stresses is controlled mainly by the orientation of bedding planes (Figure 3.9.5, Figure 3.9.9, Figure 3.9.13, Figure 3.9.17,Figure 3.9.21). The contour plots of principal stresses of each model are shown in Figure 3.9.3 to Figure 3.9.24. The very high stress concentrations are observed in the immediate vicinity of the blasthole in the models with 500 MPa blast pressure regardless of the bedding plane orientation,

but it is transferred further away in the model with double blast pressure (i.e. 1000 MPa) (Figure 3.9.15 and Figure 3.9.16).

The blast-induced fractures are generally captured between nearest bedding planes. In other words, the blast damage to the surrounding rock was limited to the same stratum where the blast took place. Since this is not the case in the model with double blast pressure, it is clear that 500 MPa blast pressure was not sufficient to grow fractures further after they intersected the bedding plane. As may be expected, the blast-induced fractures are extended by doubling the blast pressure (Figure 3.9.13). The 0 and 90 degree models showed relatively longer blast-induced fractures parallel to the bedding planes.

The displacement vector plots of each model are presented in Figure 3.9.2 to Figure 3.9.22. The maximum displacement calculated for 500 MPa models is 3 mm and for 1000 MPa model is 5 mm.

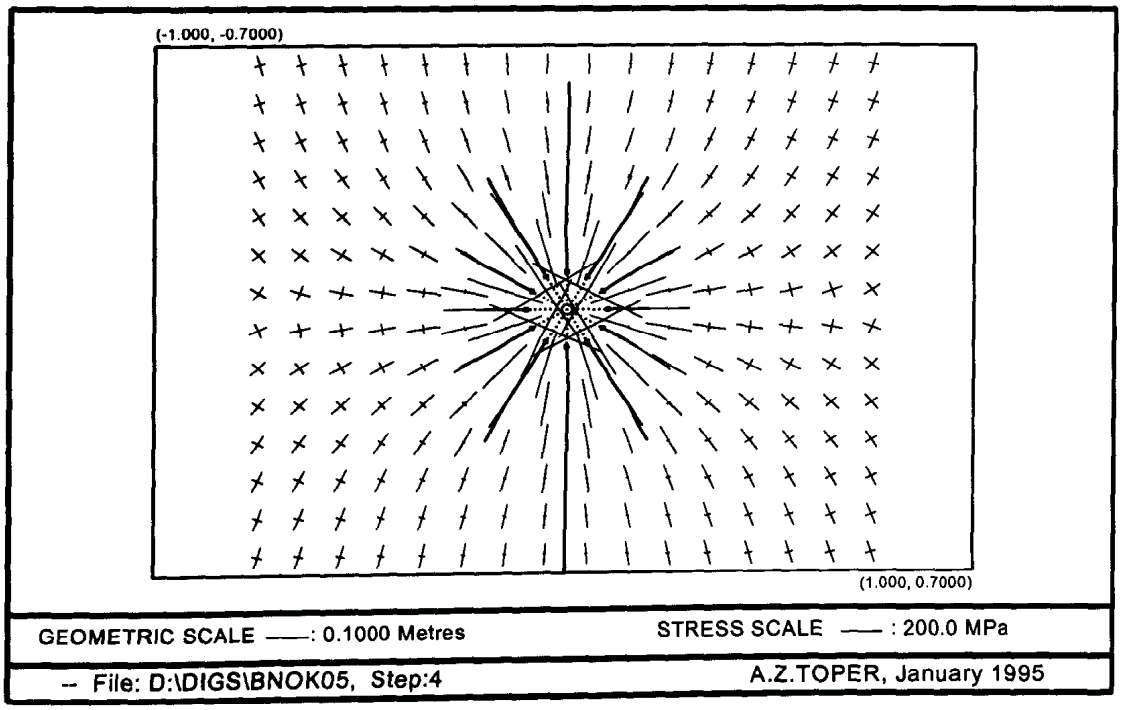

Figure 3.9.1 Plot of stress vectors (Model 1: no bedding plane, blast pressure = 500 MPa)

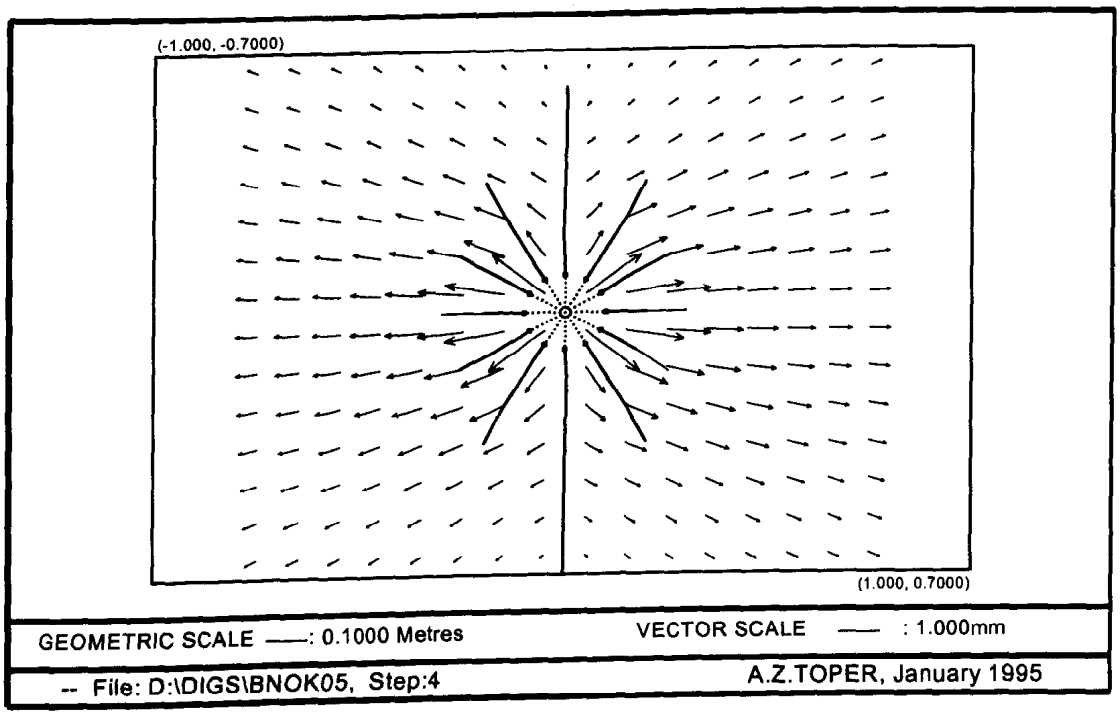

Figure 3.9.2 Plot of displacement vectors (Model 1: no bedding plane, blast pressure = 500 MPa)

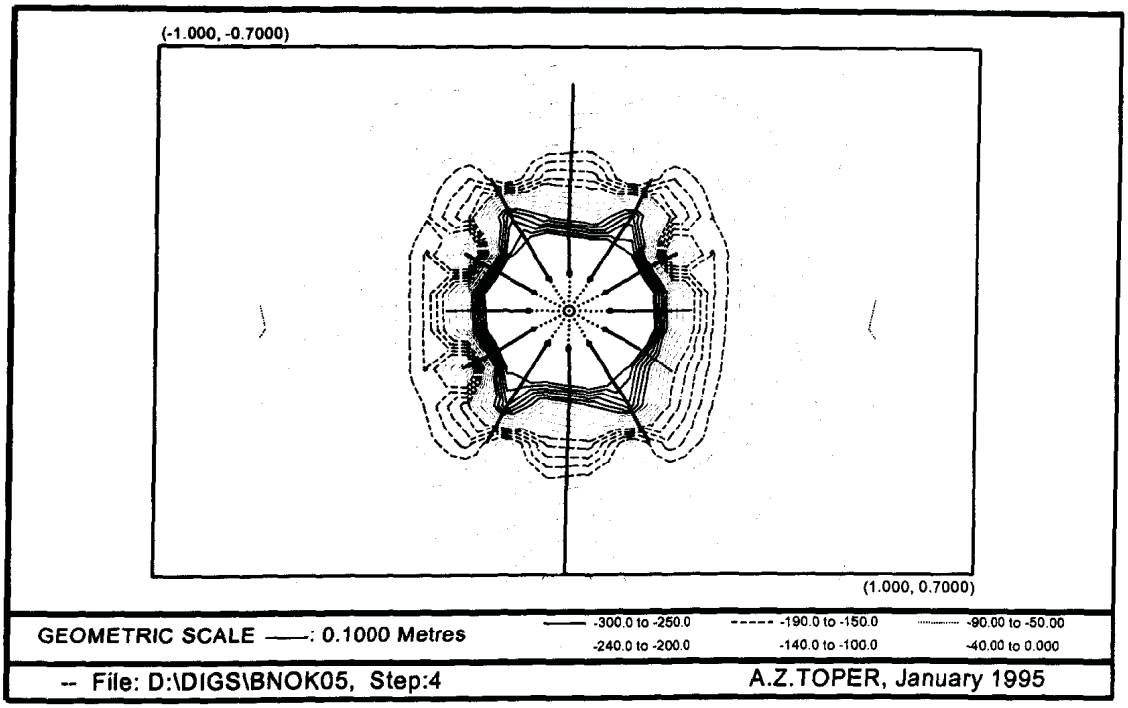

Figure 3.9.3 Plot of major principal stress contours (Model 1: no bedding plane, blast pressure = 500 MPa)

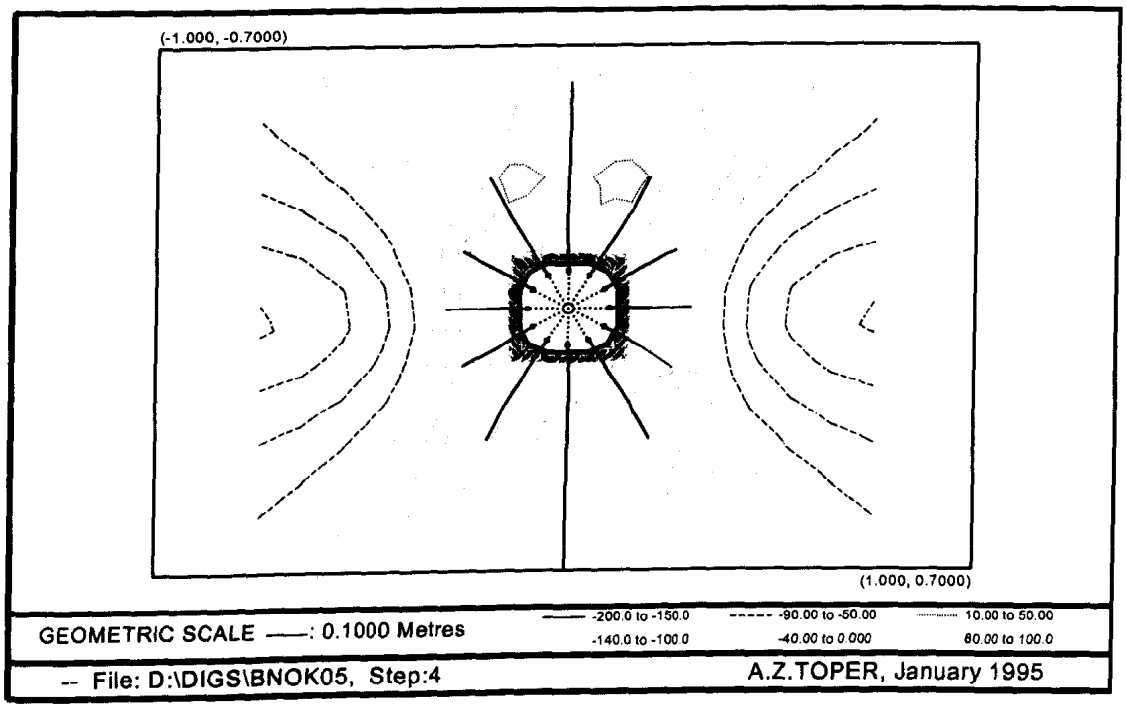

Figure 3.9.4 Plot of minor principal stress contours (Model 1: no bedding plane, blast pressure = 500 MPa)

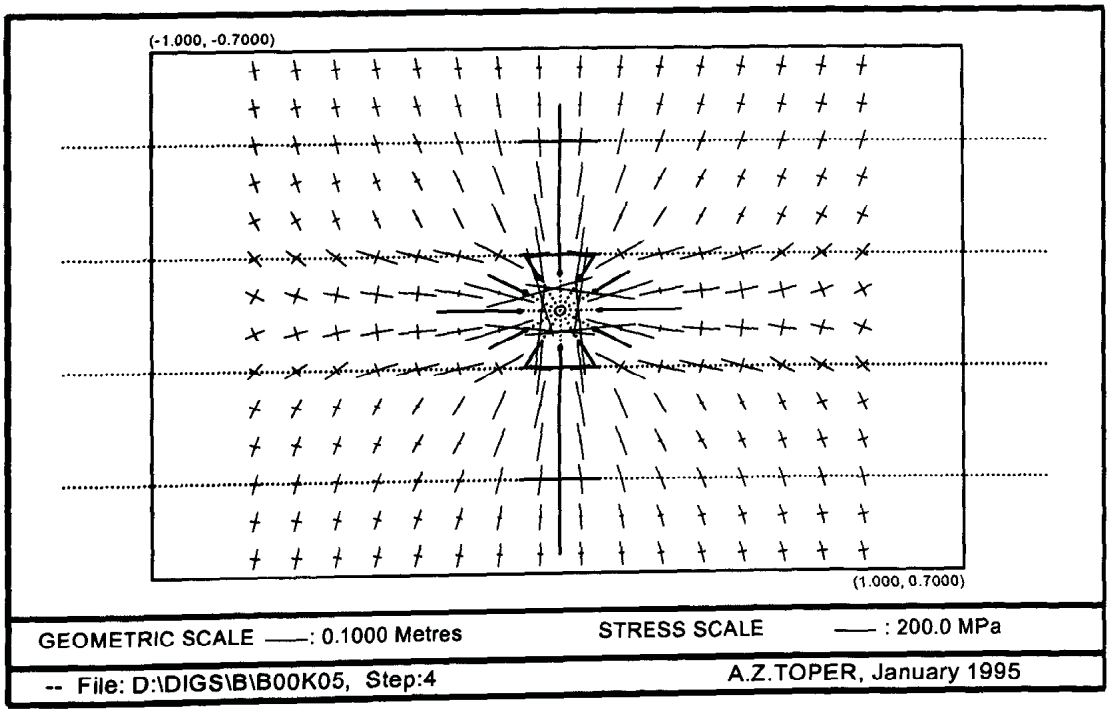

Figure 3.9.5 Plot of stress vectors (Model 2: bedding planes: 0°, blast pressure = 500 MPa)

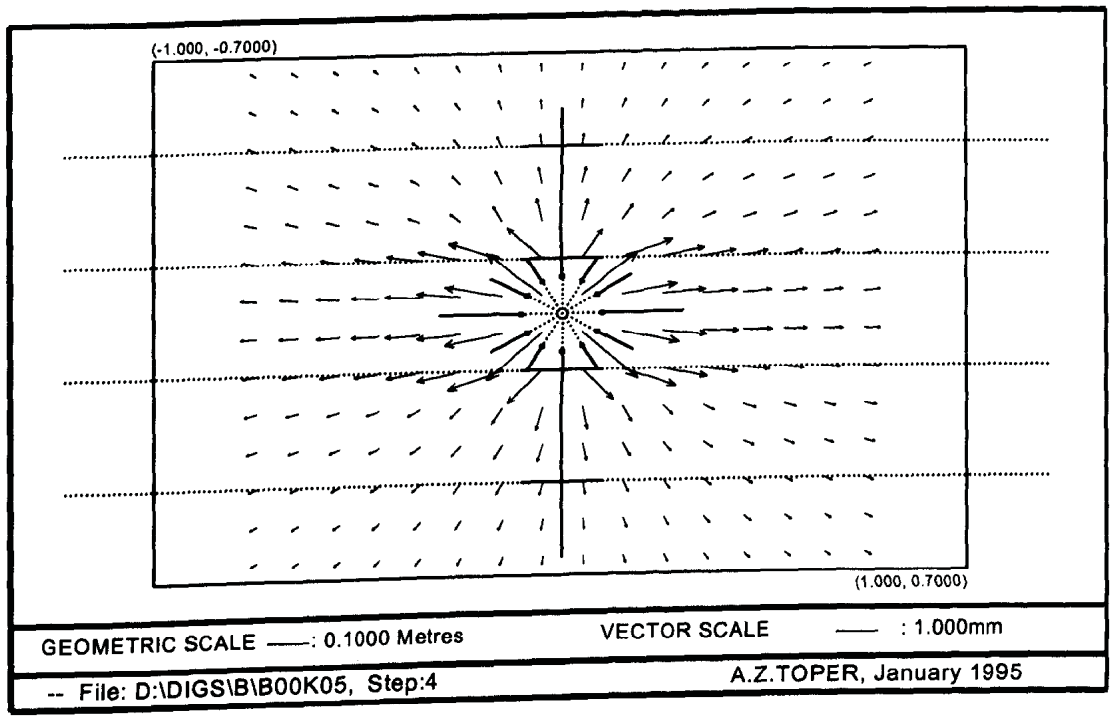

Figure 3.9.6 Plot of displacement vectors (Model 2: bedding planes: 0°, blast pressure = 500 MPa)

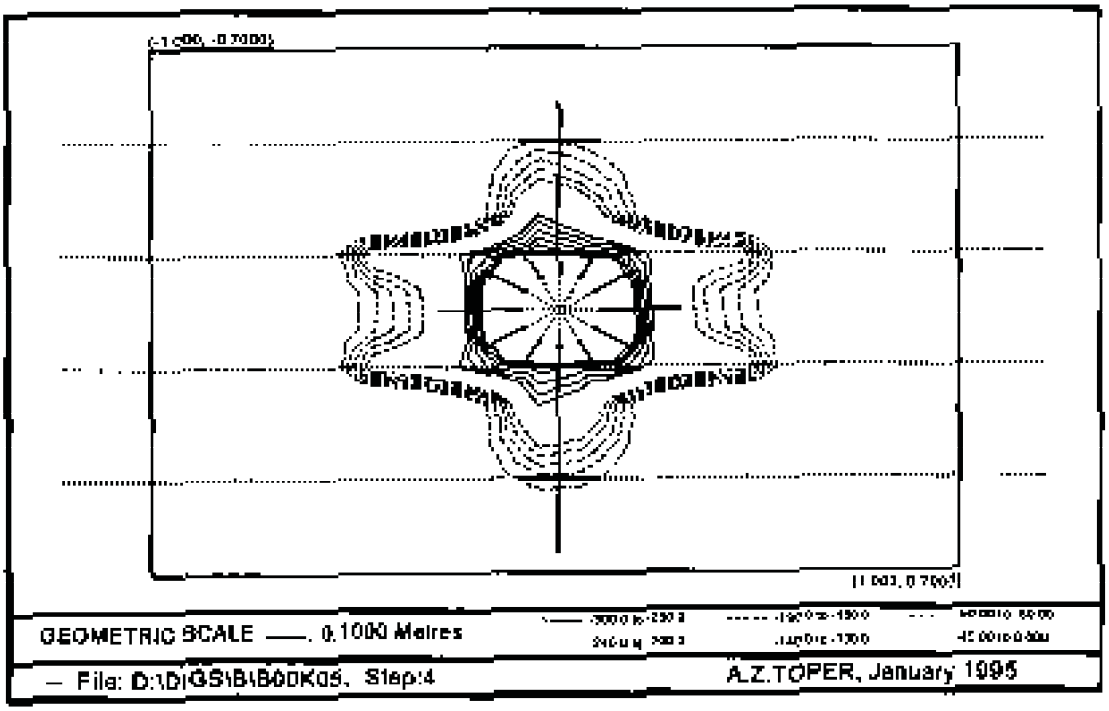

Figure 3.9.7 Plot of major principal stress contours (Model 2: bedding planes: 0°, blast pressure = 500 MPa)

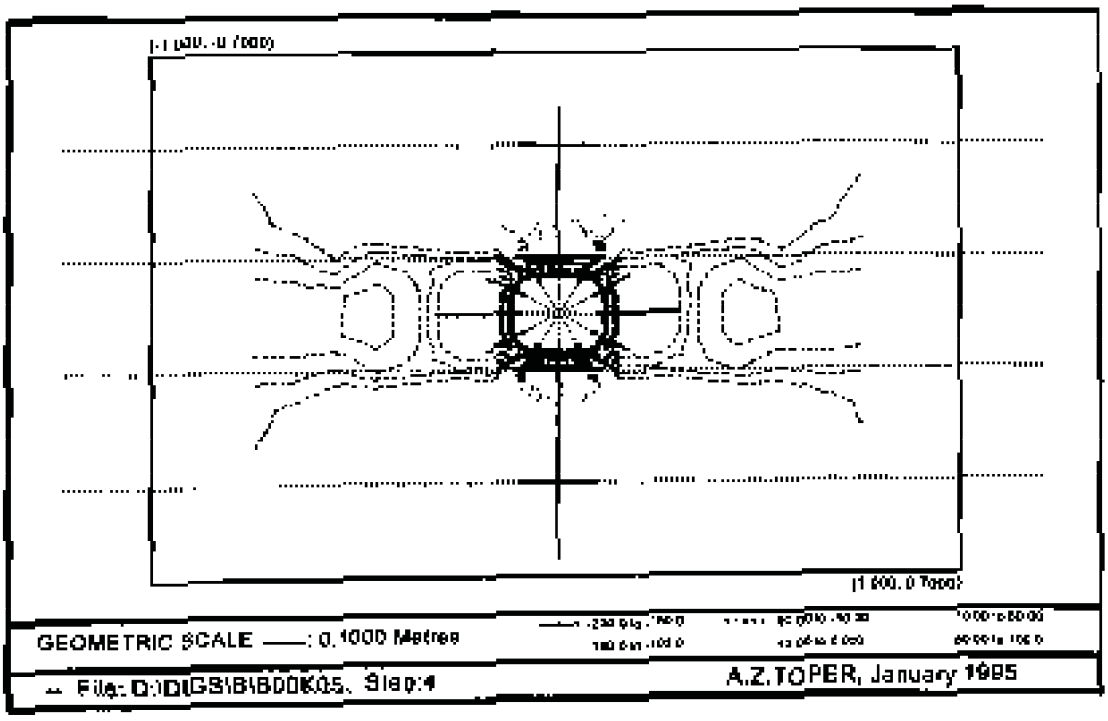

Figure 3.9.8 Plot of minor principal stress contours (Model 2: bedding planes: 0°, blast pressure = 500 MPa)

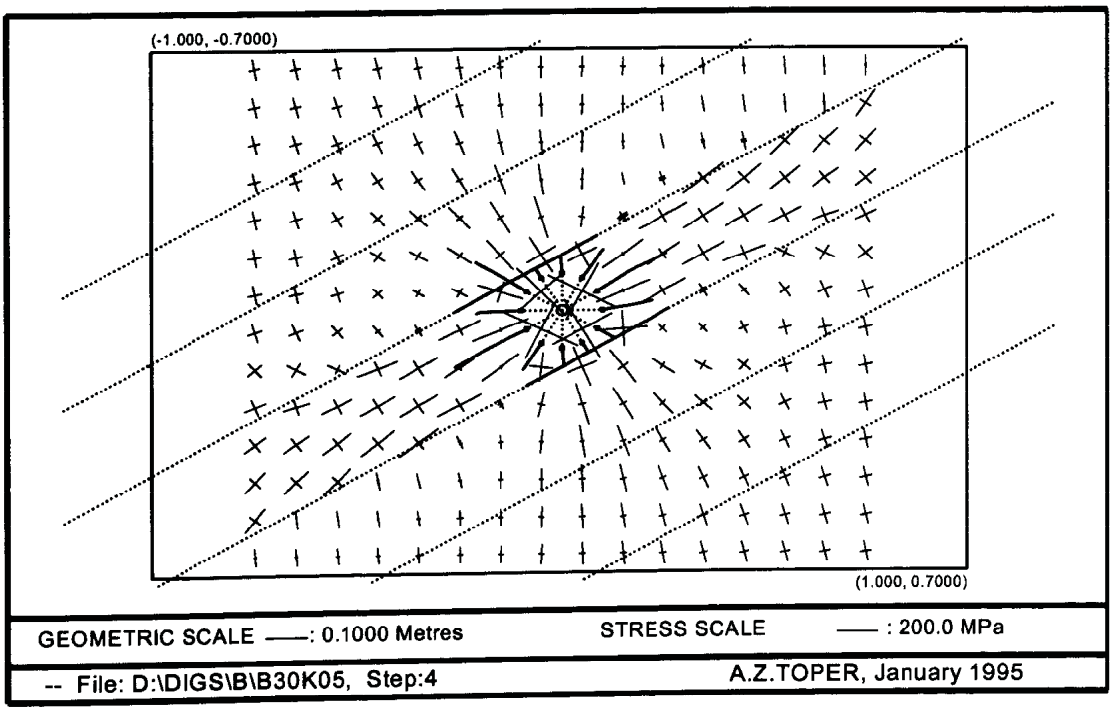

Figure 3.9.9 Plot of stress vectors (Model 3: bedding planes: 30°, blast pressure = 500 MPa)

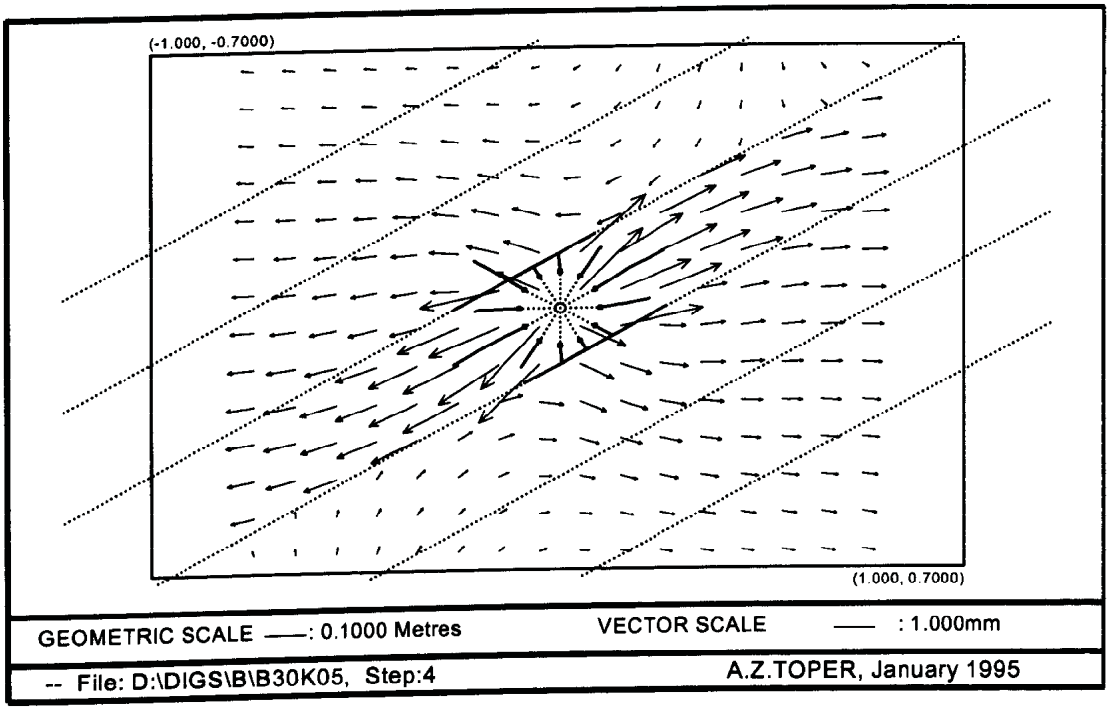

Figure 3.9.10 Plot of displacement vectors (Model 3: bedding planes: 30°, blast pressure = 500 MPa)

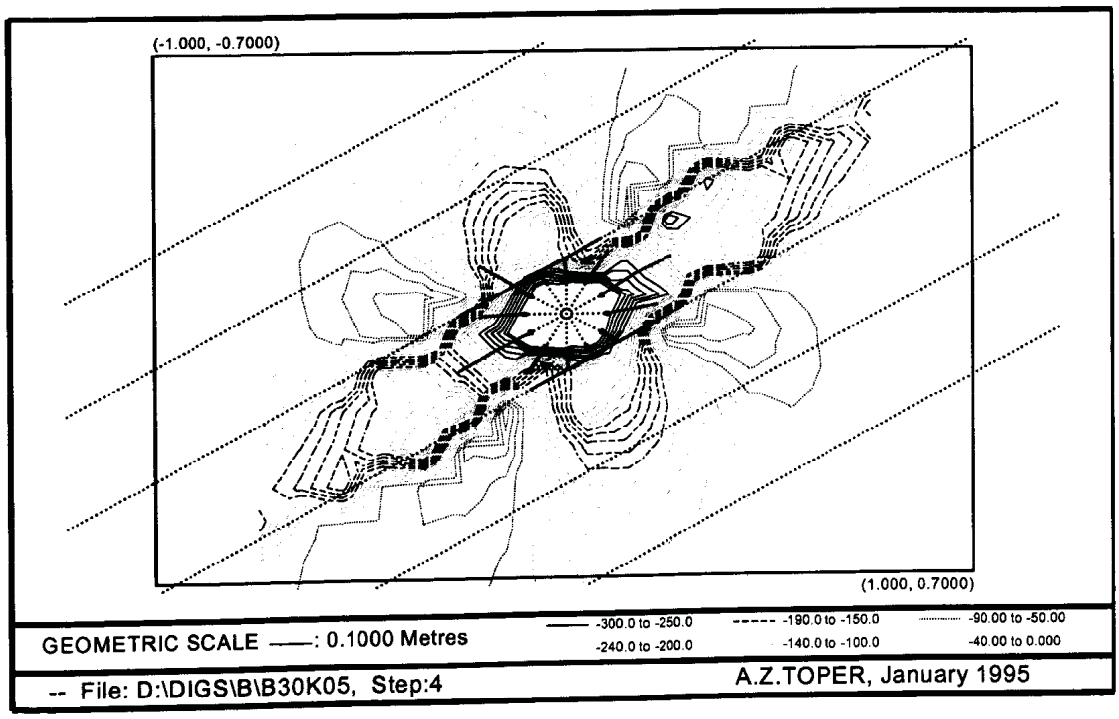

Figure 3.9.11 Plot of major principal stress contours (Model 3: bedding planes: 30°, blast pressure = 500 MPa)

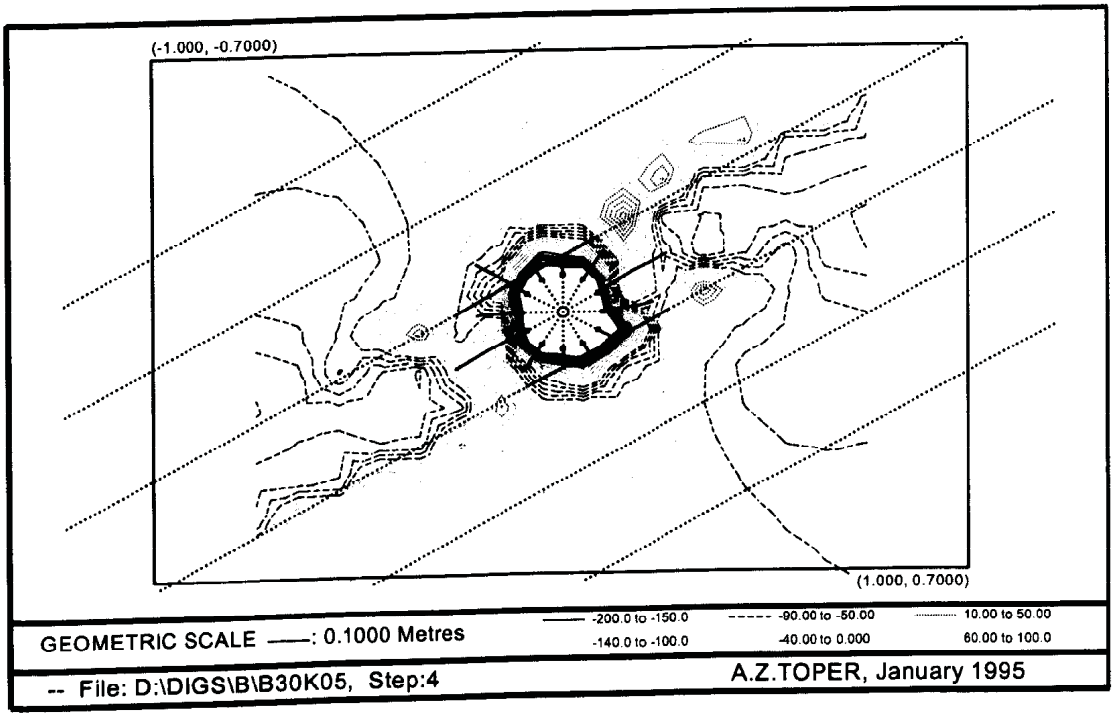

Figure 3.9.12 Plot of minor principal stress contours (Model 3: bedding planes: 30°, blast pressure = 500 MPa)

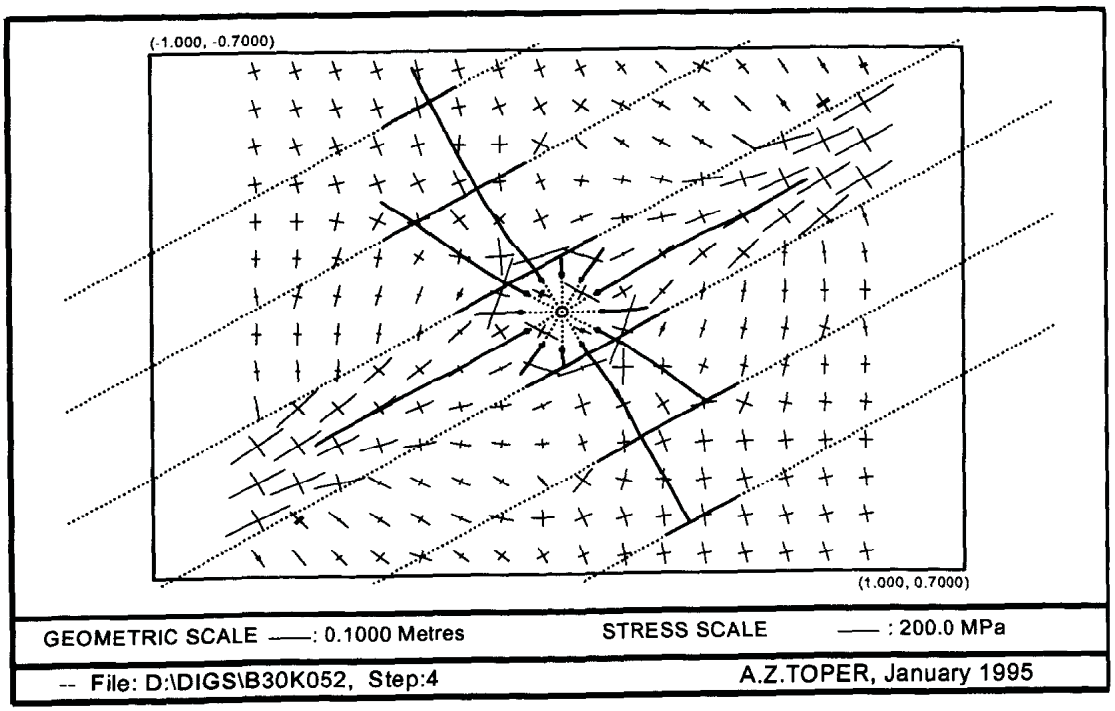

Figure 3.9.13 Plot of stress vectors (Model 4: bedding planes: 30°, blast pressure = 1000 MPa)

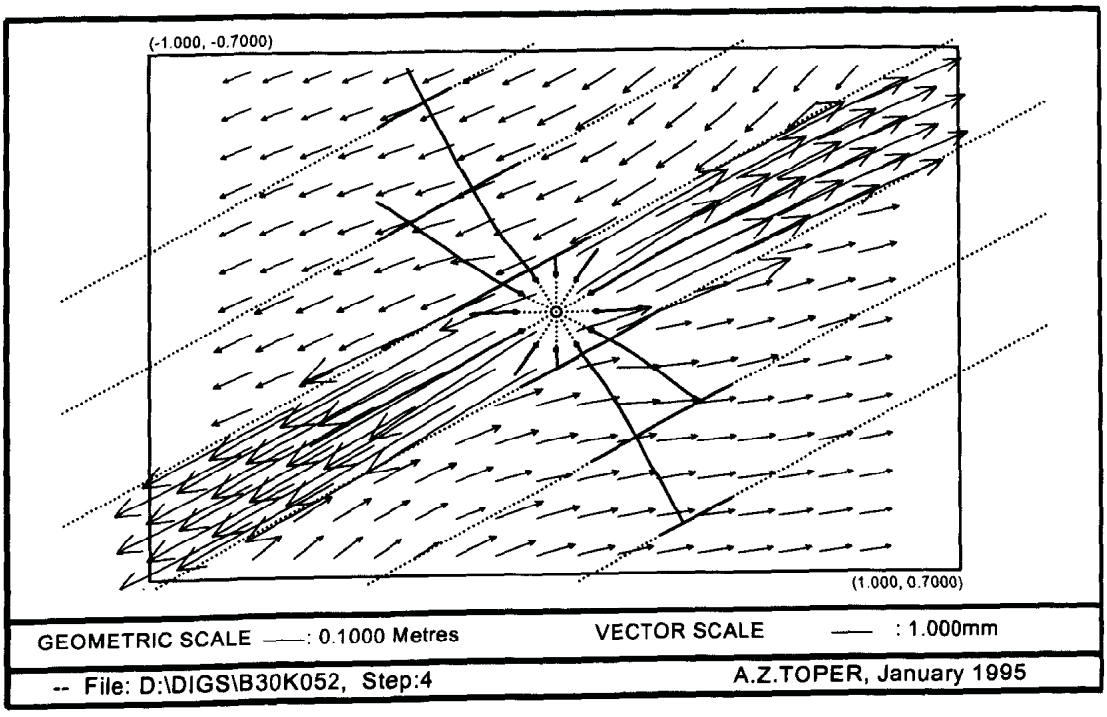

Figure 3.9.14 Plot of displacement vectors (Model 4: bedding planes: 30°, blast pressure = 1000 MPa)

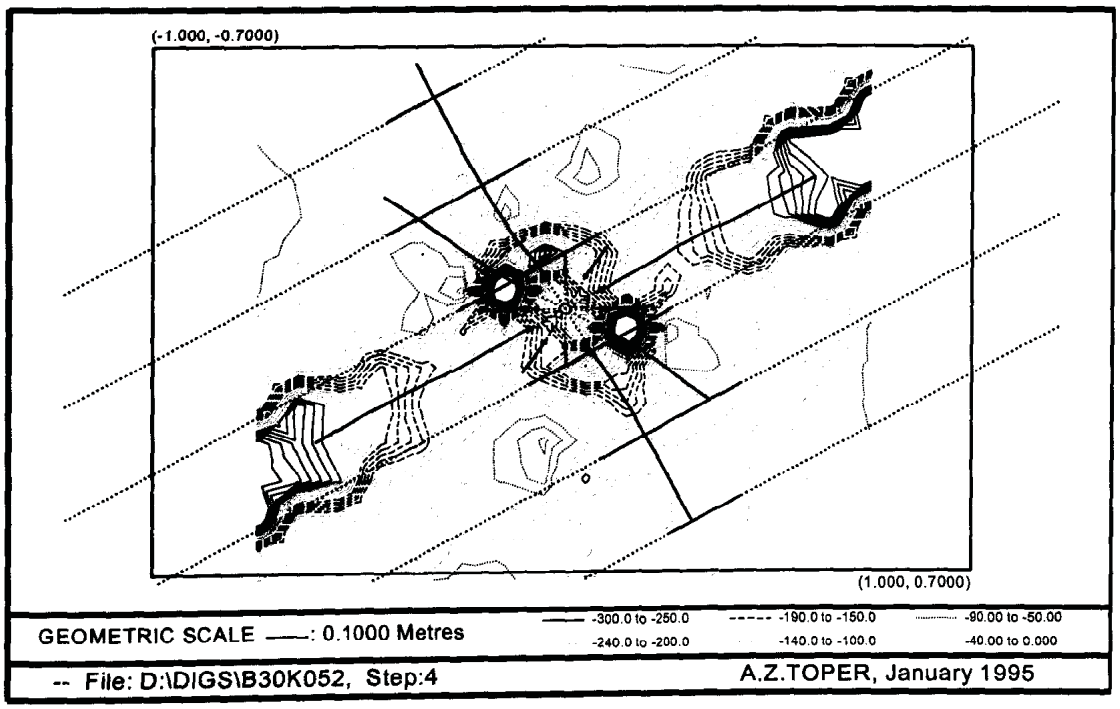

Figure 3.9.15 Plot of major principal stress contours (Model 4: bedding planes: 30°, blast pressure = 1000 MPa)

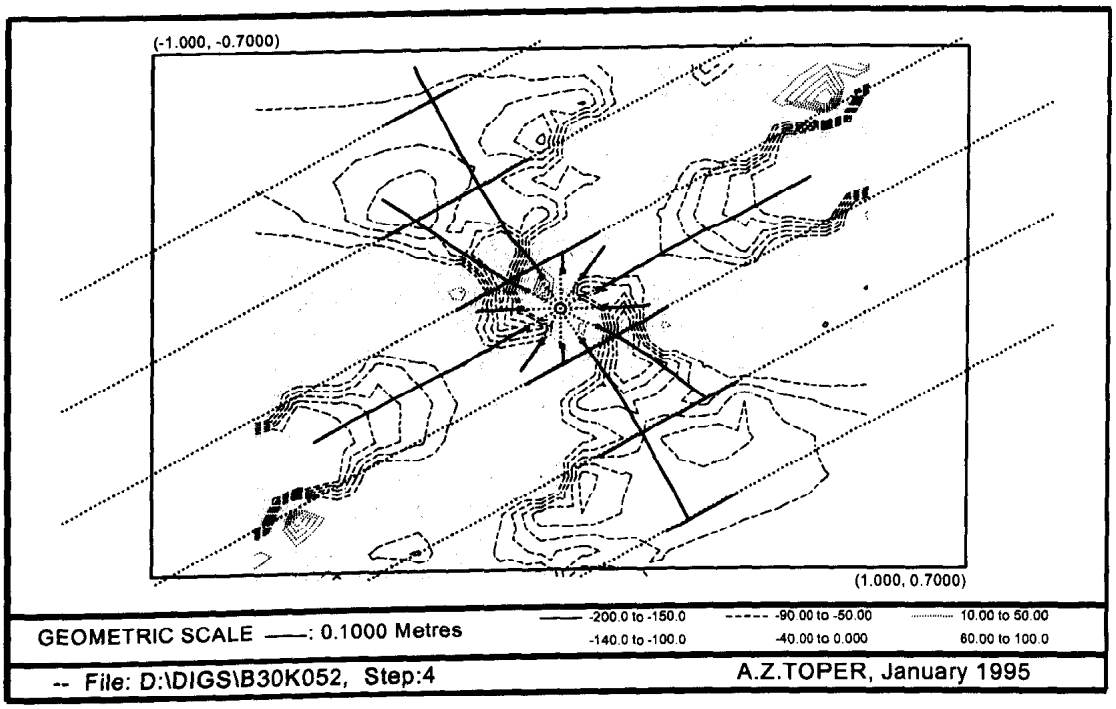

Figure 3.9.16 Plot of minor principal stress contours (Model 4: bedding planes: 30°, blast pressure = 1000 MPa)

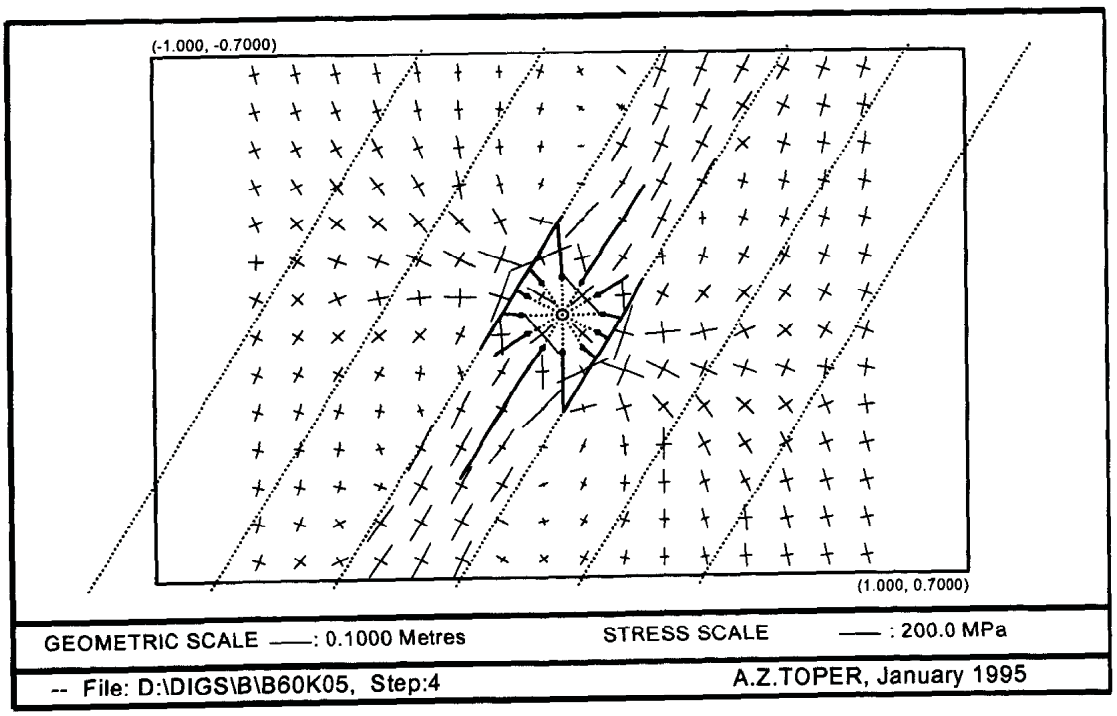

Figure 3.9.17 Plot of stress vectors (Model 5: bedding planes: 60°, blast pressure = 500 MPa)

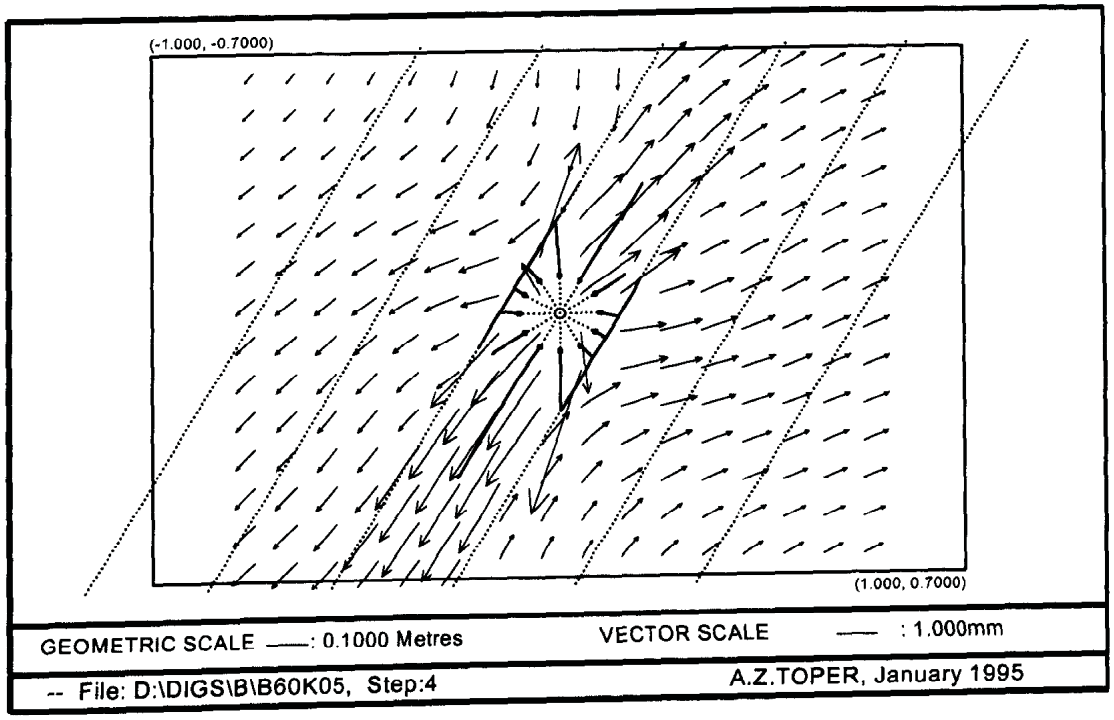

Figure 3.9.18 Plot of displacement vectors (Model 5: bedding planes: 60°, blast pressure = 500 MPa)

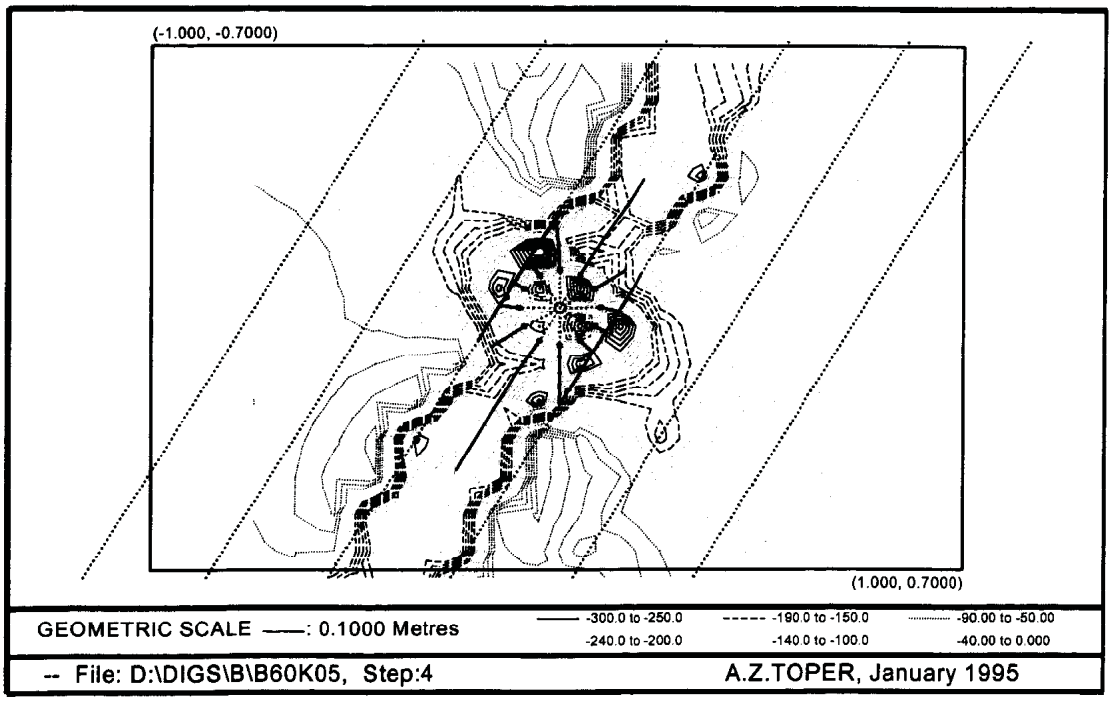

Figure 3.9.19 Plot of major principal stress contours (Model 5: bedding planes: 60°, blast pressure = 500 MPa)

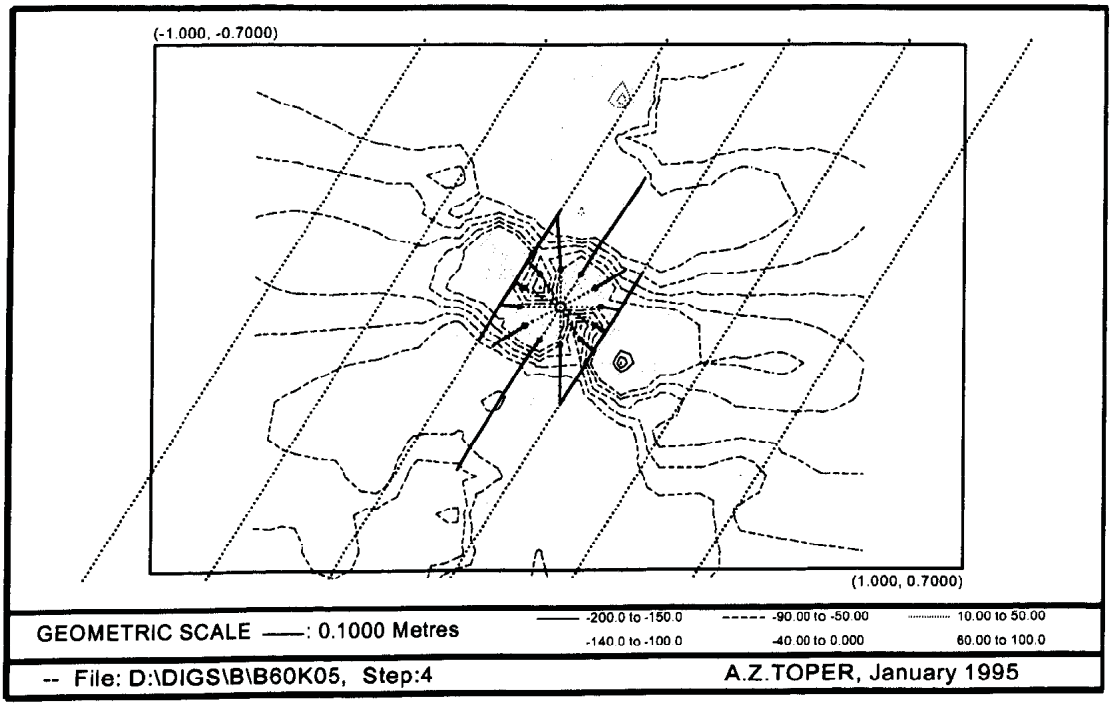

Figure 3.9.20 Plot of minor principal stress contours (Model 5: bedding planes: 60°, blast pressure = 500 MPa)

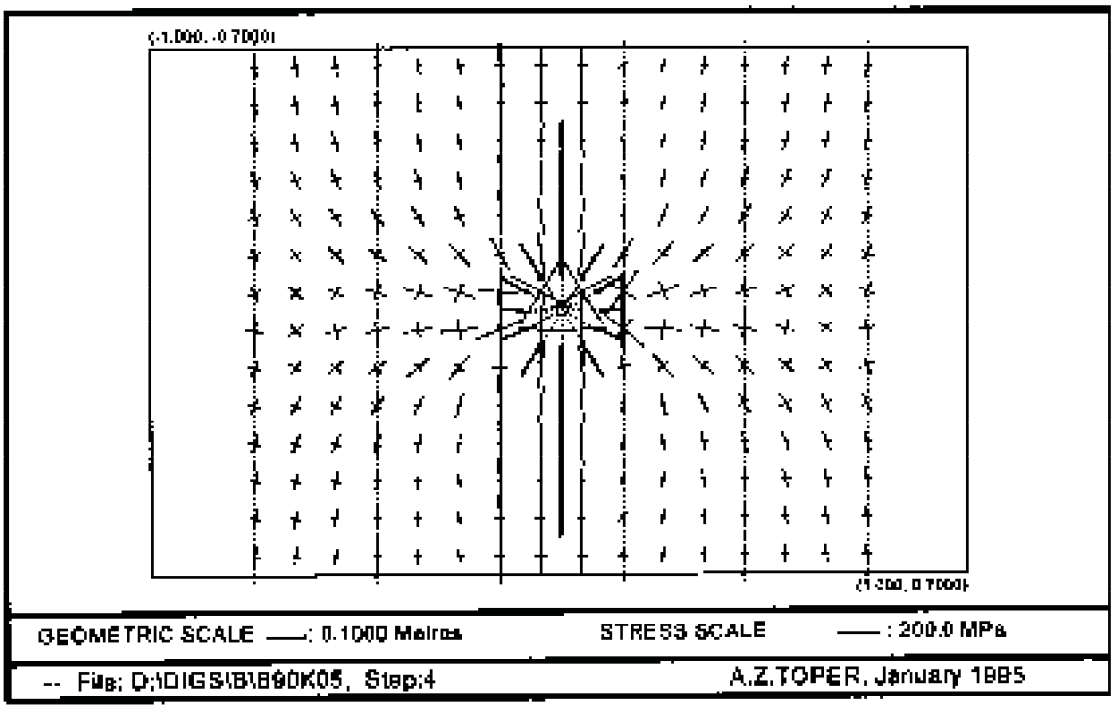

Figure 3.9.21 Plot of stress vectors (Model 6: bedding planes: 90°, blast pressure = 500 MPa)

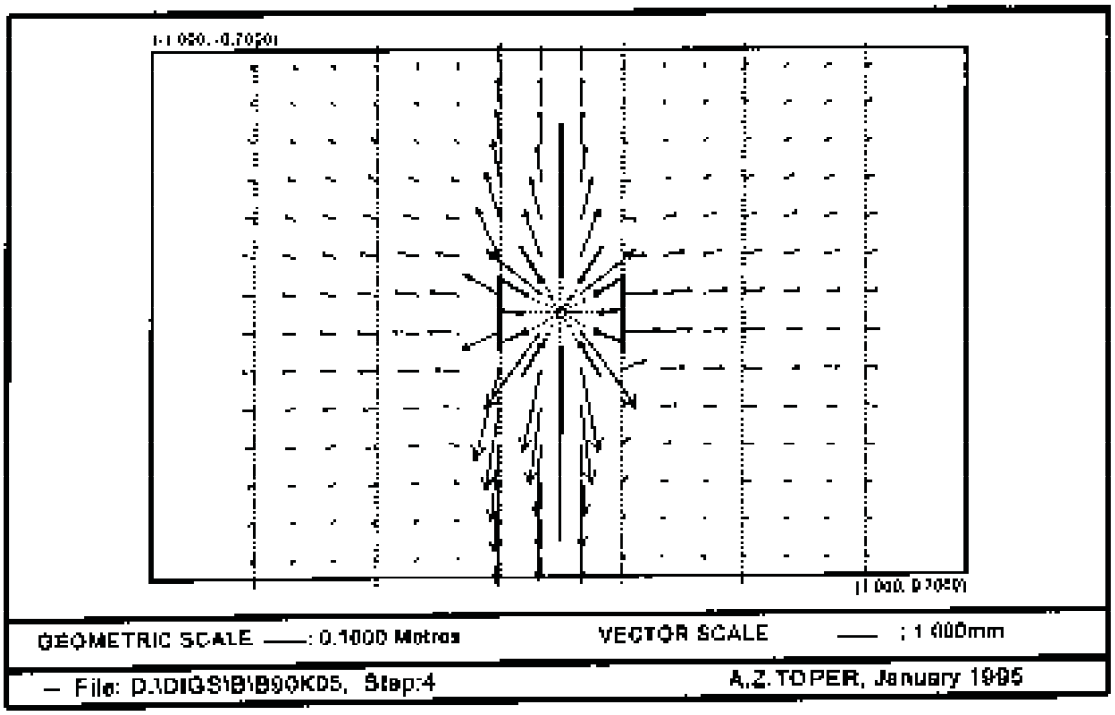

Figure 3.9.22 Plot of displacement vectors (Model 6: bedding planes: 90°, blast pressure = 500 MPa)

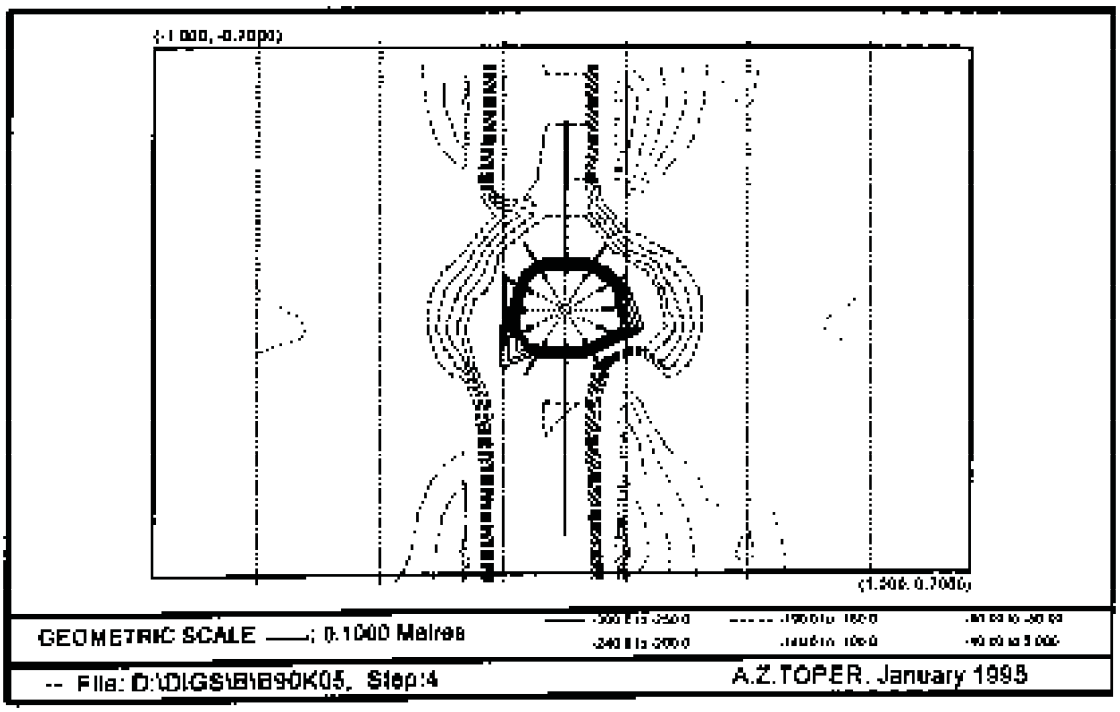

Figure 3.9.23 Plot of major principal stress contours (Model 6: bedding planes: 90°, blast pressure = 500 MPa)

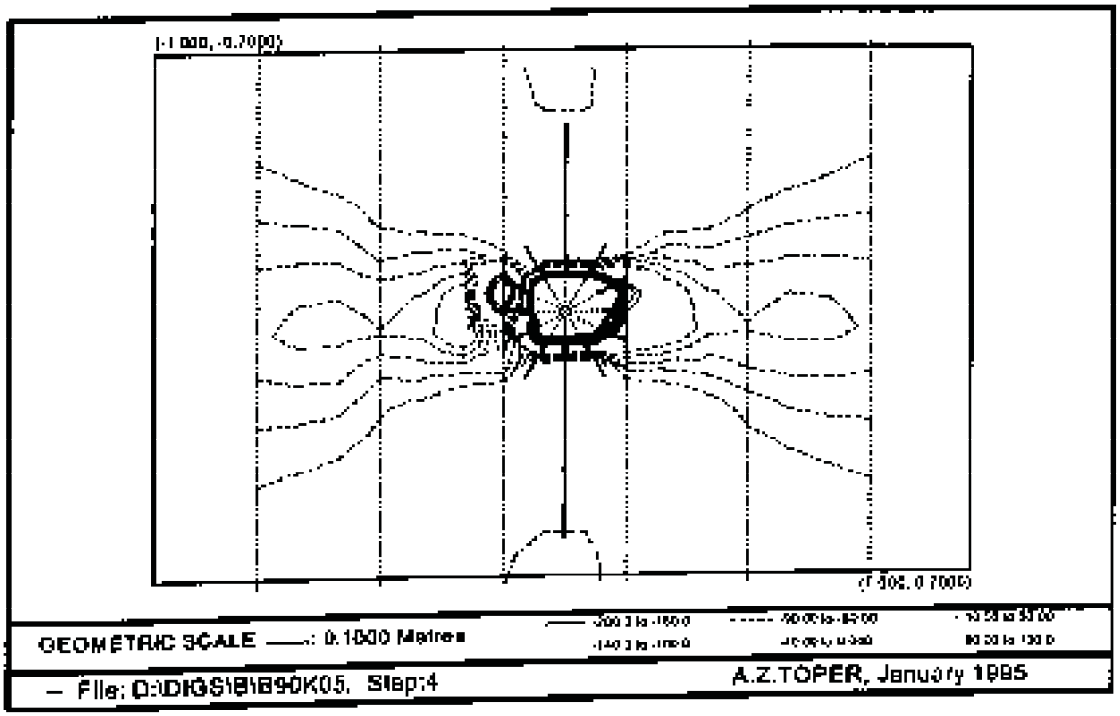

Figure 3.9.24 Plot of major principal stress contours (Model 6: bedding planes: 90°, blast pressure = 500 MPa)

3.10 Summary

The blast-induced fracturing pattern is controlled mainly by the stress field (i.e. magnitude and the orientation of principal stresses), amount of blast pressure, rock properties and the pre-existing fractures. While blasting generates new fractures, it also re-activates the pre-existing fractures and alters the stresses acting on them. Thus, the resultant fracture pattern determines the nature of the stress field in terms of magnitude and orientation of principal stresses.

Subsequent to blasting, most of the strain gauge measurements showed an increase in the major principal stresses and a decrease in the minor principal stresses. In addition to the changes in magnitudes of principal stresses, their orientations had changed as a result of the test blasts. An approximately 90 degrees re-orientation of the principal stress occurred in most of the strain-gauge measurements.

In order to investigate the effects of blasting on the surrounding rockmass and to verify the field measurements, the propagation of multiple fractures from a blasthole due to the gas pressure was simulated by very simplified numerical modelling studies. The models were designed by assuming a number of input parameters, such as the friction angle and the cohesion for the fractures, blast pressure loading and rock properties. It is a known fact that numerical modelling results are directly dependent on the input parameters used, and many numerical modelling codes have some inherit computational assumptions.

Despite the above-mentioned limitations, some of the results obtained from numerical modelling studies showed close similarities to the field observations. These similarities are set out below.

- Blasting in confined rock changes the stress field by altering the magnitude and the orientation of the principal stresses. The principal stresses are re-orientated as much as 90 degrees. This might be because of the shear movement along the bedding planes accompanying the blast and / or the residual dilation in the blasthole.

- Both models and the field measurements indicated that the effect of blasting in altering the stress field is reduced by distance from the blasthole.
- The fracture density is increased with the addition of new fractures, and the pre-existing fractures become more pronounced (widened and extended) after the blast.
- Longer blast-induced fractures were observed in the direction of maximum principal stress.
- The degree of fracture intensification is also a function of the distance to the blasthole.

Although the results obtained from the field experiments on a macro scale and the numerical modelling results show some degree of similarity, it has been recognised that current blast models are not fully satisfactory because of a lack of detailed experimental data on the microscopic scale relating to the behaviour of a confined rockmass subjected to blasting.

4 FACE-PARALLEL PRECONDITIONING

4.1 Introduction

The method of face-parallel preconditioning has been under investigation since the late 1980s, when a research project was undertaken at West Driefontein Gold Mine (Rorke *et al.*, 1989). Considerable experimentation was conducted into the drilling and blasting of 76 mm-diameter face-parallel holes positioned between 2.5 m and 3.5 m ahead of the face. A total of 18 preconditioning blasts were taken during the 11-month project. Improved hangingwall stability and a lack of damage at the face following large seismic events were reported. However, very limited instrumentation was used at the site to determine the effects of preconditioning on the rockmass. It was therefore not possible to quantify the benefits of preconditioning.

Face-parallel preconditioning was then initiated on Blyvooruitzicht Gold Mine (BMG) in the 17-24W stability pillar in September 1992, after the mining direction was changed from up-dip to breast mining. The mining configuration was overhand. Intense monitoring was carried out at the site, resulting in the formation of a geotechnical database from more than three years of mining.

Although this site provided great insight into rockmass behaviour near a stope face and into how this behaviour was affected by preconditioning, the insight was from only one site and under very specific conditions. Since mining of the pillar took place only with preconditioning, it was difficult to know how much benefit was actually gained by those blasts, as the extent to which the faces would have experienced face bursting without preconditioning was unknown.

On 30 January 1996, a rockburst from two M>2 seismic events resulted in damage to the stope, and particularly severe damage to the stope gully. The panel faces themselves remained open, with only scattered falls of ground. It was believed that preconditioning provided considerable benefit with regard to the stability of the panels in the vicinity of the stope faces. This was seen repeatedly

in other panels where events of similar magnitude occurred during the experimentation period. However, in May 1996, it was decided that the stope would be abandoned and the preconditioning experiment would come to an end, as little new information could be gained from this site.

The analysis of the geotechnical information gathered in three-and-a-half years of preconditioning experimentation in this site was reported by Lightfoot *et al.* (1996). Only a brief summary of this very comprehensive report is provided here.

4.2 Summary of findings from test site

4.2.1 Site description

The face-parallel preconditioning experiments were carried out at Blyvooruitzicht Gold Mine (BMG) in the 17-24W stability pillar (Figure 4.2.1), which was situated on the Carbon Leader Reef at a depth of over 1900 m below surface. The pillar was about 40 m wide and extended for 300 m on strike in an east / west direction. The site was very isolated; the mining faces were about 250 m from the nearest pillar and 400 m from the closest active mining. Extensive mining around the pillar has led to shearing along the top and bottom edges of the pillar, resulting in complete closure of back areas extending to the pillar itself. Support in these back areas consisted of timber packs and pipe-sticks.

4.2.2 Preconditioning layout

The 17-24W stabilising pillar was initially to be mined in the strike direction. During the establishment of the faces, a rockburst resulted in the loss of access to those breast faces. The layout was then changed to up-dip mining with 18 m-long faces and 13 m-long preconditioning holes being fanned out from the dip gullies. The drilling difficulties and damage to the collar area of the preconditioning holes, however, delayed production. In an effort to reduce these delays, a face-parallel preconditioning layout was implemented with the second

phase of up-dip mining. However, dense support and poor ground conditions resulted in poor positioning of the drill rig and, in some cases, holes were drilled 10 m ahead of the face. The blasting in such confined conditions resulted in damage to the collar of the hole and support units, which again resulted in production delays. This prompted a change in the stope layout and in September 1992, mining on strike began in conjunction with face-parallel preconditioning. This layout consisted of an advance heading at the bottom of the stope leading two panels as shown in Figure 4.2.2. Panel 2 was preconditioned from the gully in the advance heading and Panel 1 was preconditioned from the gully that is footwall lifted at the top of Panel 2. In terms of the efficiency of both preconditioning and production at the site, the change in mining layout was beneficial.

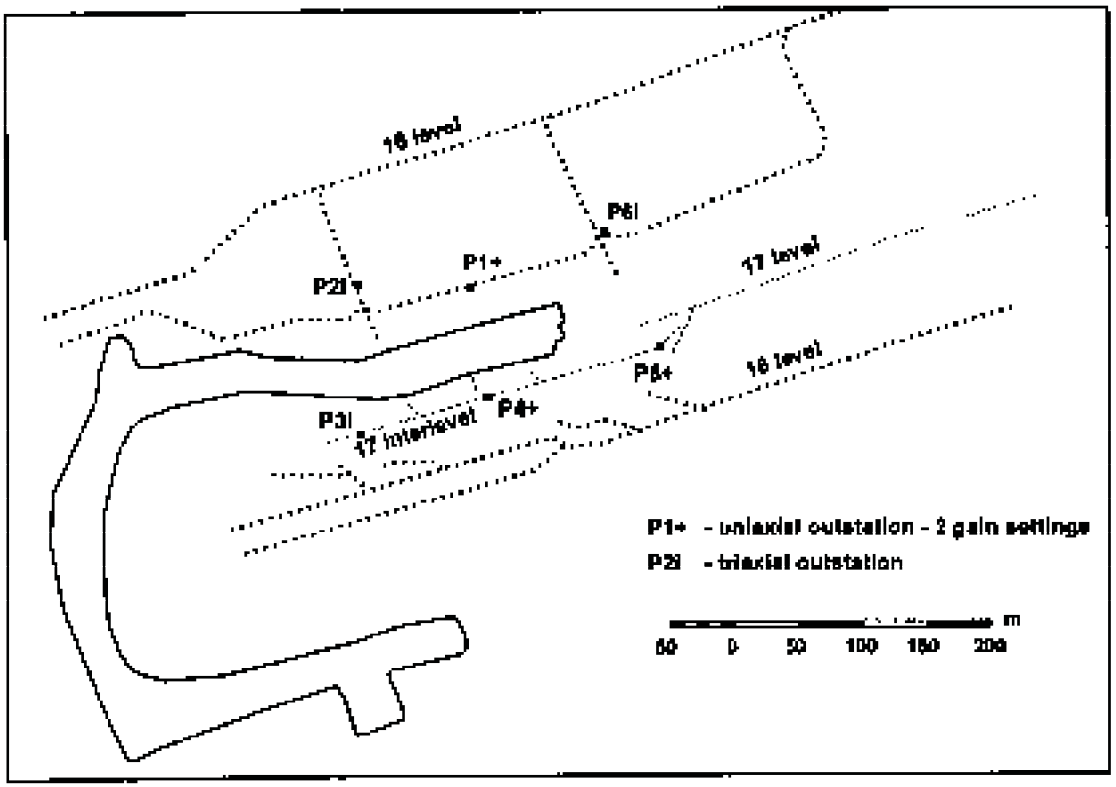

Figure 4.2.1 Plan of 17-24W stope (test site) and layout of the microseismic network around the mining faces

Panel leads of about 6.5 m were required in order for the face-parallel preconditioning holes to be drilled but this geometry had no detrimental effects on hangingwall stability. Since it was impossible to drill a face-parallel

preconditioning hole ahead of the stub, the preconditioning holes were drilled out from the stub sub-parallel to the edge of the pillar as shown in Figure 4.2.2. Although this practice was far from ideal, some reasonably good results were achieved from these blasts. The combination of 5 m of stemming from the Panel 2 preconditioning hole and the nearly 8 m of face length in the stub resulted in the bottom 13 m of the pillar not being adequately preconditioned.

4.2.3 Instrumentation and monitoring programme

Seismic coverage

A Portable Seismic System (PSS), developed at the Chamber of Mines Research Organisation (now CSIR / Miningtek), was used for the microseismic monitoring of the test site. The layout of the PSS network with respect to the 17-24W preconditioning site is shown in Figure 4.2.3. Since the preconditioning site was relatively isolated from other mining areas, the seismicity recorded from the site reflected mostly the response of the pillar to the stresses induced by the mining activities at the site, with limited external seismic influence. The horizontal extent of the network was 200 metres in the strike direction and 150 metres in the dip direction. The vertical extent was just over 30 metres and centred about the plane of the reef. Consequently, the accuracy of location of out-of-plane seismic events in the vertical direction was not as good as in the horizontal directions.

The PSS network consisted of six recording sites, these being three triaxial sites and three uniaxial sites. The system had good sensitivity, recording seismic events of magnitude down to M = -2.0 with adequate signal-to-noise ratios on most channels. Unfortunately, the PSS had a relatively limited dynamic range which resulted in saturation of the waveforms recorded at the closest sensors for events of magnitude greater than about M = 1.0. While accurate locations of such events were still possible, the magnitudes were underestimated. In these cases, reliable magnitudes for these events were obtained from Blyvooruitzicht Gold Mine's seismic network.